The Astrophysical Journal, 712:52–68, 2010 March 20 doi:10.1088/0004-637X/712/1/52
© 2010. The American Astronomical Society. All rights reserved. Printed in the U.S.A.

ON THE RELATION OF STANDARD AND HELICAL MAGNETOROTATIONAL INSTABILITY

Oleg N. Kirillov[1] and Frank Stefani[2]
[1] Dynamics and Vibrations Group, Technical University of Darmstadt, Hochschulstr. 1, 64289 Darmstadt, Germany; kirillov@dyn.tu-darmstadt.de
[2] Forschungszentrum Dresden Rossendorf, P.O. Box 510119, D-01314 Dresden, Germany; f.stefani@fzd.de
Received 2009 October 30; accepted 2010 February 1; published 2010 February 24

ABSTRACT

The magnetorotational instability (MRI) plays a crucial role for cosmic structure formation by enabling turbulence in Keplerian disks which would be otherwise hydrodynamically stable. With particular focus on MRI experiments with liquid metals, which have small magnetic Prandtl numbers, it has been shown that the helical version of this instability (HMRI) has a scaling behavior that is quite different from that of the standard MRI (SMRI). We discuss the relation of HMRI to SMRI by exploring various parameter dependencies. We identify the mechanism of transfer of instability between modes through a spectral exceptional point that explains both the transition from a stationary instability (SMRI) to an unstable traveling wave (HMRI) and the excitation of HMRI in the inductionless limit. For certain parameter regions, we find new islands of the HMRI.

Key words: accretion, accretion disks – instabilities – magnetohydrodynamics (MHD) – turbulence

1. INTRODUCTION

The magnetorotational instability (MRI; Balbus 2009) is considered as the main candidate to solve the long-standing puzzle of how stars and black holes are fed by the accretion disks surrounding them. The central problem is that these accretion disks typically rotate according to Kepler's law, $\Omega(r) \sim r^{-3/2}$, which results in an angular momentum $r^2\Omega(r) \sim r^{1/2}$. Hence, they fulfill Rayleigh's criterion stating that rotating flows with radially increasing angular momentum are hydrodynamically stable, at least in the linear sense. Such stable, non-turbulent disks would not allow the outward directed angular momentum transport that is necessary for the infalling disk matter to accrete into the central object.

In their seminal paper, Balbus & Hawley (1991) had highlighted the key role of the MRI in explaining turbulence and angular momentum transport in accretion disks around stars and black holes. They had shown that a weak, externally applied magnetic field serves only as a trigger for the instability that actually taps into the rotational energy of the flow. This is quite in contrast to current-induced instabilities, e.g., the Tayler instability (Tayler 1973), which draw their energy (at least partly) from the electric currents in the fluid.

Soon after the paper by Balbus & Hawley, it became clear that the principle mechanism of the MRI had already been revealed three decades earlier by Velikhov (1959) and Chandrasekhar (1960). Actually, they had investigated the destabilizing action of an external magnetic field for the classical Taylor–Couette (TC) flow between two concentric, rotating cylinders rather than for Keplerian rotation profile. This is, however, not a crucial difference since a TC flow can be made very close to a Keplerian one simply by adjusting the ratio of rotation rates of the inner and the outer cylinder.

The MRI in flows between rotating walls has attracted renewed interest during the last decade, mainly motivated by the increasing efforts to investigate MRI in the laboratory (Rosner et al. 2004; Stefani et al. 2008a). A first interesting experimental result was obtained in a spherical Couette flow of liquid sodium (Sisan et al. 2004). The authors observed correlated modes of velocity and magnetic field perturbation in a parameter region which is quite typical for MRI. It must be noted, however, that the background state in this spherical Couette experiment was already fully turbulent, so that the original goal that the MRI would destabilize an otherwise stable flow was not met. At Princeton University, work is going on to identify MRI in a TC experiment with liquid gallium, and first encouraging results, including the observation of nonaxisymmetric magneto–Coriolis (MC) waves, have been obtained (Nornberg 2008; Nornberg et al. 2010).

Both experiments had been designed to investigate the standard version of MRI (SMRI) with only a vertical magnetic field being applied. In this case, the azimuthal magnetic field (which is an essential ingredient of the MRI mode) must be produced from the vertical field by induction effects, which are proportional to the magnetic Reynolds number (Rm) of the flow. Rm, in turn, is proportional to the hydrodynamic Reynolds number according to $\mathrm{Rm} = \mathrm{PmRe}$, where the magnetic Prandtl number $\mathrm{Pm} = \nu/\eta$ is the ratio of viscosity ν to magnetic diffusivity $\eta = 1/\mu_0\sigma$. For liquid metals Pm is typically in the range 10^{-6}–10^{-5}. Therefore, in order to achieve $\mathrm{Rm} \sim 1$, we need $\mathrm{Re} \sim 10^5$–10^6, and wall-constrained flows (in contrast to wall-free Keplerian flows) with such high Re are usually turbulent, whatever the linear stability analysis might tell (see, however, Ji et al. 2006). This is the point which makes SMRI experiments, and their interpretation, so cumbersome.

One might ask, however, why not to substitute the induction of the necessary azimuthal magnetic field component of the MRI mode by simply externally applying this component as a part of the base configuration. Indeed, it was shown (Hollerbach & Rüdiger 2005; Rüdiger et al. 2005) that the resulting "helical MRI" (HMRI), as we now call it, is then possible at far smaller Reynolds numbers and magnetic field amplitudes than SMRI, making HMRI an ideal playground for liquid metal experiments.

First experimental evidence for HMRI was obtained in 2006 at the liquid metal facility PROMISE (Potsdam ROssendorf Magnetic InStability Experiment) which is basically a TC cell made of concentric rotating copper walls, filled with GaInSn (a eutectic which is liquid at room temperatures). In Stefani et al. (2006), Rüdiger et al. (2006), Stefani et al. (2007), and Stefani et al. (2008b), it was shown that the HMRI traveling wave appears only in the predicted finite window of the magnetic field intensity, with a frequency of the traveling wave that was also in good accordance with numerical simulations. Results of a significantly improved experiment (PROMISE 2) with strongly

reduced Ekman pumping at the end caps were published recently (Stefani et al. 2009b, 2009a).

The connection of SMRI and HMRI is presently under intense debate (Liu et al. 2006; Rüdiger & Hollerbach 2007; Priede et al. 2007; Lakhin & Velikhov 2007; Liu et al. 2007; Szklarski 2007; Rüdiger & Schultz 2008; Liu 2009; Priede & Gerbeth 2009). The first essential point to note here is that HMRI and SMRI are connected. Indeed, Figure 1 in Hollerbach & Rüdiger (2005) shows that there is a continuous and monotonic transition from HMRI to SMRI when Re and the magnetic field strength are increased simultaneously.

A second remarkable property of HMRI for small Pm (which has been coined "inductionless MRI"), was clearly worked out in Priede et al. (2007). It is the apparent paradox that a magnetic field is able to trigger an instability although the total energy dissipation of the system is larger than without this field.

The relevance of HMRI for Keplerian flows has been seriously put into question in Liu et al. (2006). Using a local WKB analysis in the small-gap approximation, the authors had shown that the HMRI works only for comparably steep rotation profiles (i.e., slightly above the Rayleigh line) and disappears for profiles as flat as the Keplerian one. This result has been confirmed by Lakhin & Velikhov (2007) and Rüdiger & Schultz (2008).

However, this disappointing result was soon relativized in Rüdiger & Hollerbach (2007) by solving the global eigenvalue equation for HMRI with various electrical boundary conditions. It turned out that HMRI re-appears again for Keplerian flows provided that at least one radial boundary is highly conducting. A similar discrepancy between local and global results is well known for the so-called stratorotational instability (SRI; Dubrulle et al. 2005) for which the existence of reflecting boundaries appears necessary for the instability to work (Umurhan 2006). This artificial demand is of course a much stronger argument against the working of SRI than the necessity of one conducting boundary is for the working of HMRI: considering, i.e., the colder outer parts of accretion disks, then the inner part can indeed be considered as a good conductor (Balbus & Henri 2008).

Other arguments that have been put forward against the relevance of HMRI for thin accretion disks are the necessity for a large ratio of toroidal to poloidal magnetic fields (Liu 2008a) and the fact that the inductionless approximation (under the assumption of finite viscosity) would lead to unphysically small values of the plasma β (Liu 2008b).

A further complication for applying HMRI to the real world is the fact that it appears in form of a traveling wave. The crucial point here is that monochromatic waves are typically not able to fulfill the axial boundary conditions at the ends of the considered region. To fulfill them, one has to consider wave packets. Only wave packets with vanishing group velocity will remain in the finite length system. Typically, the onset of this *absolute instability*, characterized by a zero growth rate *and* a zero group velocity, is harder to achieve than the *convective instability* of a monochromatic wave with zero growth rate. A comprehensive analysis of the relation of convective and absolute instability for HMRI can be found in Priede & Gerbeth (2009). From the extrapolation of the results of this paper, it seems that Keplerian rotation profiles (with conducting boundaries) are indeed absolutely HMRI-unstable, but a final solution to this puzzle is still elusive.

In the present paper, we step back from those important consideration of absolute and global instabilities and focus again on the local WKB method by considering the dispersion relation of MRI which had been derived and analyzed in Liu et al. (2006), Lakhin & Velikhov (2007), and Rüdiger & Schultz (2008). In spite of these former investigations, we feel that some points still need further clarification. This concerns a careful application of the Bilharz stability criterion as well as some further parameter dependencies, in particular the dependence for small but finite magnetic Prandtl numbers. It also concerns the question in which sense the HMRI can be considered as a *dissipation-induced instability* which is quite common in many areas of physics (Krechetnikov & Marsden 2007; Kirillov 2006, 2007).

To make the paper self-contained, we will start with a re-derivation of the dispersion relation in two forms which explicitly contain the relevant frequencies or the dimensionless parameters, respectively.

Then we will study the peculiar relation of SMRI and HMRI. As a main result of this paper we will describe in detail the mechanism of transition from SMRI to HMRI through a spectral exceptional point (EP) which appears at finite but small Pm. This provides a natural explanation for the continuous and monotonic connection between SMRI (a destabilized slow MC wave) and HMRI (a weakly destabilized inertial oscillation). In addition to this, for high Reynolds numbers we will identify a second scenario for HMRI which leads to new islands of instability at small but finite values of Pm.

2. MATHEMATICAL SETTING

In this section, we will re-derive the dispersion relation for HMRI, including viscosity and resistivity effects. Note that equivalent relations, in various forms and approximations, were already given by a number of authors (Liu et al. 2007; Lakhin & Velikhov 2007; Rüdiger et al. 2008).

The standard set of nonlinear equations of dissipative incompressible magnetohydrodynamics (Ji et al. 2001; Goodman & Ji 2002; Noguchi et al. 2002; Lakhin & Velikhov 2007; Rüdiger & Schultz 2008) consists of the Navier–Stokes equation for the fluid velocity $\mathbf{u}$,

$$\frac{\partial \mathbf{u}}{\partial t} + (\mathbf{u}\cdot\nabla)\mathbf{u} = -\frac{1}{\rho}\nabla\left(p + \frac{\mathbf{B}^2}{2\mu_0}\right) + \frac{1}{\mu_0\rho}(\mathbf{B}\cdot\nabla)\mathbf{B} + \nu\nabla^2\mathbf{u}, \quad (1)$$

and of the induction equation for the magnetic field $\mathbf{B}$,

$$\frac{\partial \mathbf{B}}{\partial t} = \nabla \times (\mathbf{u} \times \mathbf{B}) + \eta \bigtriangledown^2 \mathbf{B}, \quad (2)$$

where p is the pressure, ρ = const the density, ν = const the kinematic viscosity, $\eta = (\mu_0\sigma)^{-1}$ the magnetic diffusivity, σ is the conductivity of the fluid, and μ_0 is the magnetic permeability of free space. Additionally, the mass continuity equation for incompressible flows and the solenoidal condition for the magnetic induction yield

$$\nabla \cdot \mathbf{u} = 0, \quad \nabla \cdot \mathbf{B} = 0. \quad (3)$$

We consider the rotational fluid flow in the gap between the radii R_1 and $R_2 > R_1$, with an imposed magnetic field sustained by currents external to the fluid. The latter is important in order to distinguish the MRI from other instabilities (i.e., the Tayler instability for which electric currents are applied to the fluid). Introducing the cylindrical coordinates (R, ϕ, z), we consider the stability of a steady-state background liquid flow with the

angular velocity profile $\Omega(R)$ in helical background magnetic field (a magnetized TC flow)

$$\mathbf{u}_0 = R\,\Omega(R)\,\mathbf{e}_\phi, \quad p = p_0(R), \quad \mathbf{B}_0 = B_\phi^0(R)\mathbf{e}_\phi + B_z^0\mathbf{e}_z, \quad (4)$$

with the azimuthal component

$$B_\phi^0(R) = \frac{\mu_0 I}{2\pi R}, \quad (5)$$

which can be thought of as being produced by an axial current I. The angular velocity profile of the background TC flow is

$$\Omega(R) = a + \frac{b}{R^2}, \quad (6)$$

where a and b are arbitrary constants as in TC experiments (Wendl 1999). The centrifugal acceleration of the background flow (Equation (6)) is compensated by the pressure gradient (Ji et al. 2001):

$$R\Omega^2 = \frac{1}{\rho}\frac{\partial p_0}{\partial R}. \quad (7)$$

2.1. Linearization with Respect to Axisymmetric Perturbations

Throughout the paper, we will restrict our interest to axisymmetric perturbations $\mathbf{u}' = \mathbf{u}'(R, z)$, $\mathbf{B}' = \mathbf{B}'(R, z)$, and $p' = p'(R, z)$ about the stationary solution (Equations (4)–(7)), keeping in mind that for strongly dominant azimuthal magnetic fields also nonaxisymmetric perturbations are possible (Hollerbach et al. 2010).

With the notation

$$D_1 = \partial_R\partial_R^\dagger + \partial_z^2, \quad D_2 = \partial_R^\dagger\partial_R + \partial_z^2, \quad (8)$$

where the differential operators are defined in Equation (A1), the general linearized Equations (A2) derived in the Appendix are simplified in the assumption of axisymmetric perturbations to

$$\begin{aligned}
&(\partial_t - \nu D_1)u_R' - 2\Omega u_\phi' \\
&\quad = -\frac{1}{\rho}\left[\partial_R p' + \frac{1}{\mu_0}\left(B_z^0\partial_R B_z' + B_\phi^0\partial_R B_\phi'\right)\right] \\
&\qquad + \frac{1}{\mu_0\rho}\left(B_z^0\partial_z B_R' - \frac{B_\phi^0}{R}B_\phi'\right), \\
&(\partial_t - \nu D_1)u_\phi' + \frac{\kappa^2}{2\Omega}u_R' = \frac{B_z^0}{\mu_0\rho}\partial_z B_\phi', \\
&(\partial_t - \nu D_2)u_z' = -\frac{1}{\rho}\left[\partial_z p' + \frac{1}{\mu_0}\left(B_z^0\partial_z B_z' \right.\right. \\
&\qquad \left.\left. + B_\phi^0\partial_z B_\phi'\right)\right] + \frac{B_z^0}{\mu_0\rho}\partial_z B_z', \\
&(\partial_t - \eta D_1)B_R' = B_z^0\partial_z u_R', \\
&(\partial_t - \eta D_1)B_\phi' = B_z^0\partial_z u_\phi' + \frac{2B_\phi^0}{R}u_R' + (R\partial_R\Omega)B_R', \\
&(\partial_t - \eta D_2)B_z' = -B_z^0\partial_R^\dagger u_R', \\
&\partial_z u_z' = -\partial_R^\dagger u_R', \\
&\partial_z B_z' = -\partial_R^\dagger B_R', \quad (9)
\end{aligned}$$

where the squared epicyclic frequency κ is defined as

$$\kappa^2 = 2\Omega\left(2\Omega + R\frac{d\Omega}{dR}\right) = \frac{1}{R^3}\frac{d}{dR}(\Omega^2 R^4). \quad (10)$$

Following the approach of Goodman & Ji (2002) and Liu et al. (2006), we act on the first of Equations (9) by the operator $\partial_R^\dagger$ and on the third one by the operator ∂_z. Summing the results, taking into account that

$$\partial_R^\dagger D_1 = D_2\partial_R^\dagger, \quad \partial_R^\dagger B_\phi^0 = 0, \quad \partial_R(B_\phi^0 B_\phi') = -\frac{B_\phi^0 B_\phi'}{R} + B_\phi^0\partial_R B_\phi', \quad (11)$$

and using the last two equations of Equations (9) yields

$$\begin{aligned}
-2\Omega\partial_R^\dagger u_\phi' &= -\frac{1}{\rho}D_2\left[p' + \frac{1}{\mu_0}B_z^0 B_z'\right] \\
&\quad - \frac{1}{\rho}\frac{1}{\mu_0}\left(\partial_R^\dagger B_\phi^0\partial_R + \partial_z^2 B_\phi^0\right)B_\phi' \\
&\quad - \frac{1}{\mu_0\rho}\partial_R^\dagger\left(\frac{B_\phi^0}{R}B_\phi'\right) \\
&= -\frac{1}{\rho}D_2\left[p' + \frac{1}{\mu_0}\left(B_z^0 B_z' + B_\phi^0 B_\phi'\right)\right] \\
&\quad - \frac{2}{\mu_0\rho}\partial_R^\dagger\left(\frac{B_\phi^0}{R}B_\phi'\right). \quad (12)
\end{aligned}$$

Therefore, we extend the identity obtained in Goodman & Ji (2002) to the case $B_\phi^0 \neq 0$:

$$D_2\frac{1}{\rho}\left[p' + \frac{1}{\mu_0}\left(B_z^0 B_z' + B_\phi^0 B_\phi'\right)\right] = 2\partial_R^\dagger\left(\Omega u_\phi' - \frac{1}{\mu_0\rho}\frac{B_\phi^0}{R}B_\phi'\right). \quad (13)$$

On the other hand, using Equation (11), we transform the first of Equations (9) into

$$\begin{aligned}
(\partial_t - \nu D_1)u_R' - 2\Omega u_\phi' = &-\partial_R\frac{1}{\rho}\left[p' + \frac{1}{\mu_0}\left(B_z^0 B_z' + B_\phi^0 B_\phi'\right)\right] \\
&+ \frac{1}{\mu_0\rho}\left(B_z^0\partial_z B_R' - \frac{2B_\phi^0}{R}B_\phi'\right). \quad (14)
\end{aligned}$$

Acting on both sides of Equation (14) by the operator D_1 and taking into account the identity (13) and

$$D_1\partial_R = \left(\partial_R\partial_R^\dagger + \partial_z^2\right)\partial_R = \partial_R\left(\partial_R^\dagger\partial_R + \partial_z^2\right) = \partial_R D_2, \quad (15)$$

we get

$$\begin{aligned}
&D_1(\partial_t - \nu D_1)u_R' - 2\Omega D_1 u_\phi' \\
&\quad = -\partial_R D_2\frac{1}{\rho}\left[p' + \frac{1}{\mu_0}\left(B_z^0 B_z' + B_\phi^0 B_\phi'\right)\right] \\
&\qquad + D_1\frac{1}{\mu_0\rho}\left(B_z^0\partial_z B_R' - \frac{2B_\phi^0}{R}B_\phi'\right) \\
&\quad = -2\partial_R\partial_R^\dagger\left(\Omega u_\phi' - \frac{1}{\mu_0\rho}\frac{B_\phi^0}{R}B_\phi'\right) \\
&\qquad + D_1\frac{1}{\mu_0\rho}\left(B_z^0\partial_z B_R' - \frac{2B_\phi^0}{R}B_\phi'\right). \quad (16)
\end{aligned}$$

Rearranging the terms and using the definition of the operator D_1 yields

$$
\begin{aligned}
&D_1(\partial_t - \nu D_1)u'_R - 2\Omega\partial_z^2 u'_\phi \\
&\quad = 2\partial_R\partial_R^\dagger \frac{1}{\mu_0\rho}\frac{B_\phi^0}{R}B'_\phi + \frac{1}{\mu_0\rho}B_z^0 D_1\partial_z B'_R - \frac{1}{\mu_0\rho}D_1\frac{2B_\phi^0}{R}B'_\phi \\
&\quad = \frac{1}{\mu_0\rho}B_z^0 D_1\partial_z B'_R - \frac{1}{\mu_0\rho}\frac{2B_\phi^0}{R}\partial_z^2 B'_\phi. \qquad (17)
\end{aligned}
$$

Therefore, we have separated the equations for u'_R, u'_ϕ, and B'_R, B'_ϕ from the others in Equations (9):

$$
\begin{aligned}
(\partial_t - \nu D_1)D_1 u'_R - 2\Omega\partial_z^2 u'_\phi &= \frac{1}{\mu_0\rho}B_z^0 D_1\partial_z B'_R \\
&\quad - \frac{1}{\mu_0\rho}\frac{2B_\phi^0}{R}\partial_z^2 B'_\phi, \\
(\partial_t - \nu D_1)u'_\phi + \frac{\kappa^2}{2\Omega}u'_R &= \frac{B_z^0}{\mu_0\rho}\partial_z B'_\phi, \\
(\partial_t - \eta D_1)B'_R &= B_z^0\partial_z u'_R, \\
(\partial_t - \eta D_1)B'_\phi &= B_z^0\partial_z u'_\phi + \frac{2B_\phi^0}{R}u'_R + (R\partial_R\Omega)B'_R. \qquad (18)
\end{aligned}
$$

Note that after introducing the stream functions for the poloidal components

$$
u'_R = \partial_z\varphi, \quad u'_z = -\partial_R^\dagger\varphi, \quad B'_R = \partial_z\psi, \quad B'_z = -\partial_R^\dagger\psi, \qquad (19)
$$

Equations (18) extend the inviscid equations of Liu et al. (2006) to the case $\nu \neq 0$.

We can rewrite Equations (18) in the form of the operator matrix equation $\partial_t\tilde{E}\xi' = \tilde{H}\xi'$, where $\xi' = (u'_R, u'_\phi, B'_R, B'_\phi)^T$,

$$
\tilde{E} = \begin{pmatrix} D_1 & 0 & 0 & 0 \\ 0 & 1 & 0 & 0 \\ 0 & 0 & 1 & 0 \\ 0 & 0 & 0 & 1 \end{pmatrix},
$$

$$
\tilde{H} = \begin{pmatrix} \nu D_1^2 & 2\Omega\partial_z^2 & \frac{B_z^0}{\mu_0\rho}D_1\partial_z & -\frac{2B_\phi^0}{\mu_0\rho R}\partial_z^2 \\ -\frac{\kappa^2}{2\Omega} & \nu D_1 & 0 & \frac{B_z^0}{\mu_0\rho}\partial_z \\ B_z^0\partial_z & 0 & \eta D_1 & 0 \\ \frac{2B_\phi^0}{R} & B_z^0\partial_z & R\partial_R\Omega & \eta D_1 \end{pmatrix}. \qquad (20)
$$

The resulting multiparameter family of operator matrices equipped with boundary conditions can be investigated by numerical or perturbative (Kirillov et al. 2009; Kirillov 2010) methods. In the following, we use the local WKB approximation.

2.2. Local WKB Approximation

We choose a fiducial point (R_0, z_0), around which we perform the local stability analysis (Pessah & Psaltis 2005). We expand all the background quantities in Taylor series around (R_0, z_0) and retain only the zeroth order in terms of the local coordinates $\tilde{R} = R - R_0$ and $\tilde{z} = z - z_0$ to obtain the operator matrix equation with the constant coefficients

$$
\partial_t\tilde{E}_0\xi' = \tilde{H}_0\xi' \qquad (21)
$$

with

$$
\tilde{E}_0 = \begin{pmatrix} D_1^0 & 0 & 0 & 0 \\ 0 & 1 & 0 & 0 \\ 0 & 0 & 1 & 0 \\ 0 & 0 & 0 & 1 \end{pmatrix},
$$

$$
\tilde{H}_0 = \begin{pmatrix} \nu(D_1^0)^2 & 2\Omega_0\partial_{\tilde{z}}^2 & \frac{B_z^0}{\mu_0\rho}D_1^0\partial_{\tilde{z}} & -\frac{2B_\phi^0}{\mu_0\rho R_0}\partial_{\tilde{z}}^2 \\ -\frac{\kappa_0^2}{2\Omega_0} & \nu D_1^0 & 0 & \frac{B_z^0}{\mu_0\rho}\partial_{\tilde{z}} \\ B_z^0\partial_{\tilde{z}} & 0 & \eta D_1^0 & 0 \\ \frac{2B_\phi^0}{R_0} & B_z^0\partial_{\tilde{z}} & \frac{\kappa_0^2}{2\Omega_0} - 2\Omega_0 & \eta D_1^0 \end{pmatrix}, \qquad (22)
$$

where

$$
\begin{aligned}
&\Omega_0 = \Omega(R_0), \quad \kappa_0^2 = 2\Omega_0\left(2\Omega_0 + R_0\left.\frac{d\Omega}{dR}\right|_{R=R_0}\right), \\
&B_\phi^0 = B_\phi^0(R_0), \quad D_1^0 = \partial_{\tilde{R}}^2 + \partial_{\tilde{z}}^2 + \frac{\partial_{\tilde{R}}}{R_0} - \frac{1}{R_0^2}. \qquad (23)
\end{aligned}
$$

Equation (21) is a linear PDE with the constant coefficients in the local variables $(\tilde{R}, \tilde{z})$ for the perturbed quantities ξ'. This is a good approximation as long as the variations $\tilde{R}$ and $\tilde{z}$ are small in comparison with the characteristic length scales in the radial and vertical directions, respectively (Pessah & Psaltis 2005). A solution to Equation (21) has the form of a plane wave:

$$
\xi' = \tilde{\xi}\exp(\gamma t + ik_R\tilde{R} + ik_z\tilde{z}), \quad \tilde{\xi} = (\tilde{u}_R, \tilde{u}_\phi, \tilde{B}_R, \tilde{B}_\phi)^T, \qquad (24)
$$

where $\tilde{\xi}$ is a vector of constant coefficients.

Introducing the total wavenumber $k^2 = k_z^2 + k_R^2$ and denoting $\alpha = k_z/k$, we find

$$
\begin{aligned}
&D_1^0\exp(\gamma t + ik_R\tilde{R} + ik_z\tilde{z}) \\
&\quad = \left(-k^2 + \frac{ik_R}{R_0} - \frac{1}{R_0^2}\right)\exp(\gamma t + ik_R\tilde{R} + ik_z\tilde{z}). \qquad (25)
\end{aligned}
$$

In the WKB approximation, we restrict the analysis to the modes with the wavenumbers satisfying $k_R R_0 \gg 1$ which allows us to neglect the terms $\frac{ik_R}{R_0} - \frac{1}{R_0^2}$ in Equation (25). In view of this, after substitution of Equation (24) into Equation (21), we arrive at the matrix eigenvalue problem:

$$
(H - \gamma E)\tilde{\xi} = 0, \qquad (26)
$$

with E as a unit matrix and $H = -\mathrm{diag}(\omega_\nu, \omega_\nu, \omega_\eta, \omega_\eta) + H_1 + H_2$, where $\omega_\nu = \nu k^2$ and $\omega_\eta = \eta k^2$ are the viscous and resistive frequencies,

$$
H_1 = \frac{i\omega_A}{\sqrt{\mu_0\rho}}\begin{pmatrix} 0 & 0 & 1 & 0 \\ 0 & 0 & 0 & 1 \\ \mu_0\rho & 0 & 0 & 0 \\ 0 & \mu_0\rho & 0 & 0 \end{pmatrix}, \qquad (27)
$$

$$
H_2 = \begin{pmatrix} 0 & 2\Omega_0\alpha^2 & 0 & -2\omega_{A_\phi}\frac{\alpha^2}{\sqrt{\mu_0\rho}} \\ -2\Omega_0 - R_0\left.\frac{d\Omega}{dR}\right|_{R=R_0} & 0 & 0 & 0 \\ 0 & 0 & 0 & 0 \\ -2\omega_{A_\phi}\sqrt{\mu_0\rho} & 0 & R_0\left.\frac{d\Omega}{dR}\right|_{R=R_0} & 0 \end{pmatrix}, \qquad (28)
$$

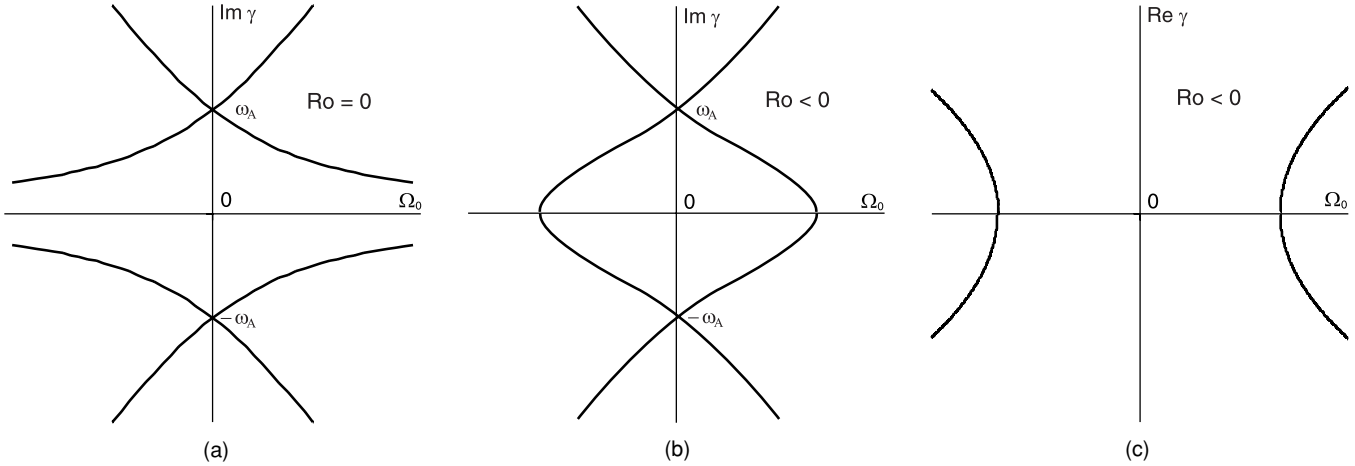

Figure 1. (a) Coriolis splitting of the Alfvén plane wave into the fast and the slow magneto–Coriolis (MC) waves, (b) shear causes interaction of slow MC branches with the origination of the double zero eigenvalue, and (c) splitting of the double zero eigenvalue yields positive real eigenvalues (SMRI).

and the Alfvén frequencies are

$$\omega_A^2 = \frac{k_z^2 \left(B_z^0\right)^2}{\mu_0 \rho}, \quad \omega_{A_\phi}^2 = \frac{\left(B_\phi^0\right)^2}{\mu_0 \rho R_0^2}. \tag{29}$$

Note that the matrix $-\mathrm{diag}(\omega_\nu, \omega_\nu, \omega_\eta, \omega_\eta) + H_1$ has two double eigenvalues related to the damped Alfvén modes (Nornberg et al. 2010):

$$\gamma_{1,2} = -\frac{\omega_\nu + \omega_\eta}{2} + \sqrt{\left(\frac{\omega_\nu - \omega_\eta}{2}\right)^2 - \omega_A^2},$$
$$\gamma_{3,4} = -\frac{\omega_\nu + \omega_\eta}{2} - \sqrt{\left(\frac{\omega_\nu - \omega_\eta}{2}\right)^2 - \omega_A^2}. \tag{30}$$

When $\omega_{A_\phi} = 0$, $\frac{d\Omega}{dR}\big|_{R=R_0} = 0$, the eigenvalues of the matrix $H_1 + H_2$ correspond to the Alfvén-inertial or MC waves (Lehnert 1954)

$$\gamma_{1,2} = i\sqrt{\omega_A^2 + \Omega_0^2 \alpha^2} \pm i\alpha\Omega_0,$$
$$\gamma_{3,4} = -i\sqrt{\omega_A^2 + \Omega_0^2 \alpha^2} \pm i\alpha\Omega_0. \tag{31}$$

Figure 1(a) demonstrates how rotation leads to the splitting of plane Alfvén waves into the fast and slow MC waves (Lehnert 1954). The system with purely imaginary eigenvalues (Equation (31)) is marginally stable and its destabilization, caused by dissipation, shear, or azimuthal magnetic fields, can efficiently be treated by methods that were developed in the theory of dissipation-induced instabilities (Krechetnikov & Marsden 2007; Kirillov 2007, 2009).

On the other hand, the matrix H can be considered as a result of a non-Hermitian complex perturbation $H_1 + H_2$ of a real symmetric matrix, which has two double semi-simple eigenvalues–diabolical points (Berry & Dennis 2003). This is a typical situation for the problems of wave propagation in chiral absorptive media (Keck et al. 2003; Berry & Dennis 2003; Kirillov et al. 2005) or in rotating symmetric continua (Kirillov 2009).

2.3. Dispersion Relation in Terms of Dimensionless Parameters

The stability of the propagating plane wave perturbation (Equation (25)) is determined by the roots γ of the dispersion relation,

$$P(\gamma) = \gamma^4 + a_1\gamma^3 + a_2\gamma^2 + (a_3 + ib_3)\gamma + a_4 + ib_4 = 0, \tag{32}$$

where $P(\gamma) = \det(H - \gamma E)$. We write the coefficients of the complex polynomial (Equation (32)) in the form

$$\begin{aligned}
a_1 &= 2(\omega_\nu + \omega_\eta),\\
a_2 &= (\omega_\nu + \omega_\eta)^2 + 2\left(\omega_A^2 + \omega_\nu\omega_\eta\right) + \alpha^2\kappa_0^2 + 4\alpha^2\omega_{A_\phi}^2,\\
a_3 &= 2(\omega_\eta + \omega_\nu)\left(\omega_A^2 + \omega_\eta\omega_\nu\right) + 2\alpha^2\kappa_0^2\omega_\eta + 4\alpha^2(\omega_\eta + \omega_\nu)\omega_{A_\phi}^2,\\
a_4 &= \left(\omega_A^2 + \omega_\nu\omega_\eta\right)^2 - 4\alpha^2\omega_A^2\Omega_0^2 + \alpha^2\kappa_0^2\left(\omega_A^2 + \omega_\eta^2\right)\\
&\quad + 4\alpha^2\omega_\nu\omega_\eta\omega_{A_\phi}^2,\\
b_3 &= -8\alpha^2\Omega_0\omega_A\omega_{A_\phi},\\
b_4 &= -4\alpha^2\Omega_0\omega_A\omega_{A_\phi}(2\omega_\eta + \omega_\nu) - \kappa_0^2\alpha^2\Omega_0^{-1}\omega_A\omega_{A_\phi}(\omega_\eta - \omega_\nu).
\end{aligned} \tag{33}$$

After scaling the spectral parameter as $\gamma = \lambda\sqrt{\omega_\nu\omega_\eta}$, we express the appropriately normalized coefficients (Equation (33)) by means of the dimensionless Rossby number (Ro), magnetic Prandtl number (Pm), ratio of the Alfvén frequencies (β^*), Hartmann (Ha*), and Reynolds (Re*) numbers:

$$\mathrm{Ro} = \frac{1}{2}\frac{R_0}{\Omega_0}\frac{d\Omega}{dR}\bigg|_{R=R_0}, \quad \mathrm{Pm} = \frac{\nu}{\eta} = \frac{\omega_\nu}{\omega_\eta}, \quad \beta^* = \alpha\frac{\omega_{A_\phi}}{\omega_A},$$
$$\mathrm{Re}^* = \alpha\frac{\Omega_0}{\omega_\nu}, \quad \mathrm{Ha}^* = \alpha\frac{B_z^0}{k\sqrt{\mu_0\rho\nu\eta}}. \tag{34}$$

Additional transformations yield the coefficients of the dispersion relation $P(\lambda) = 0$ in a simplified form:

$$\begin{aligned}
a_1 &= 2\left(\sqrt{\mathrm{Pm}} + \frac{1}{\sqrt{\mathrm{Pm}}}\right),\\
a_2 &= \frac{a_1^2}{4} + 2(1 + \mathrm{Ha}^{*2}) + 4\beta^{*2}\mathrm{Ha}^{*2} + 4\mathrm{Re}^{*2}\mathrm{Pm}(1 + \mathrm{Ro}),\\
a_3 &= a_1(1 + \mathrm{Ha}^{*2}) + 2a_1\beta^{*2}\mathrm{Ha}^{*2} + 8\mathrm{Re}^{*2}(1 + \mathrm{Ro})\sqrt{\mathrm{Pm}},\\
a_4 &= (1 + \mathrm{Ha}^{*2})^2 + 4\beta^{*2}\mathrm{Ha}^{*2} + 4\mathrm{Re}^{*2}\\
&\quad + 4\mathrm{Re}^{*2}\mathrm{Ro}(\mathrm{Pm}\mathrm{Ha}^{*2} + 1),\\
b_3 &= -8\beta^*\mathrm{Ha}^{*2}\mathrm{Re}^*\sqrt{\mathrm{Pm}},\\
b_4 &= -4\beta^*\mathrm{Ha}^{*2}\mathrm{Re}^*(2 + (1 - \mathrm{Pm})\mathrm{Ro}).
\end{aligned} \tag{35}$$

Therefore, we have exactly reproduced the dispersion relation of Lakhin & Velikhov (2007) and Rüdiger & Schultz (2008), which generalizes that of Goodman & Ji (2002) and Liu et al. (2006).

3. SMRI IN THE ABSENCE OF THE AZIMUTHAL MAGNETIC FIELD ($\beta^* = 0$)

Let us first assume $\beta^* = 0$ and study the onset of the SMRI. The coefficients of the polynomial $P(\lambda)$ are then real because $b_3 = 0$ and $b_4 = 0$. We have

$$\begin{aligned} a_1 &= \hat{a}_1 = 2\left(\sqrt{\mathrm{Pm}} + \frac{1}{\sqrt{\mathrm{Pm}}}\right), \\ a_2 &= \hat{a}_2 = \frac{\hat{a}_1^2}{4} + 2(1 + \mathrm{Ha}^{*2}) + 4\mathrm{Re}^{*2}\mathrm{Pm}(1 + \mathrm{Ro}), \\ a_3 &= \hat{a}_3 = \hat{a}_1(1 + \mathrm{Ha}^{*2}) + 8\mathrm{Re}^{*2}(1 + \mathrm{Ro})\sqrt{\mathrm{Pm}}, \\ a_4 &= \hat{a}_4 = (1 + \mathrm{Ha}^{*2})^2 + 4\mathrm{Re}^{*2}(1 + \mathrm{Ro}(\mathrm{PmHa}^{*2} + 1)). \end{aligned} \tag{36}$$

Composing the Hurwitz matrix of the real polynomial $P(\lambda)$, we write the Lienard and Chipart criterion of asymptotic stability (Lienard & Chipart 1914; Marden 1966): all roots λ have $\mathrm{Re}\lambda < 0$ if and only if

$$\begin{aligned} &\hat{a}_4 > 0, \quad \hat{a}_2 > 0, \quad h_1 = \hat{a}_1 > 0, \\ &h_3 = \hat{a}_1\hat{a}_2\hat{a}_3 - \hat{a}_1^2\hat{a}_4 - \hat{a}_3^2 > 0. \end{aligned} \tag{37}$$

Explicit calculation of h_3 shows that it is a sum of squared quantities:

$$\begin{aligned} h_3 = 64&\left(\mathrm{Pm}^*\mathrm{Re}^{*2}(\mathrm{Ro} + 1) + \frac{\hat{a}_1^2}{16}\right)^2 \\ &+ \mathrm{Ha}^{*2}\hat{a}_1^2\left(\frac{\hat{a}_1^2}{4} + 4\mathrm{Re}^{*2}\right) > 0. \end{aligned} \tag{38}$$

Therefore, the condition $h_3 > 0$ is always fulfilled.

The local definition of the Rossby number (Equation (34)) allows us to vary it for the background profile $\Omega(R) = a + bR^{-2}$ changing the coefficients a and b because $\mathrm{Ro} = -b/(aR_0^2 + b)$. On the other hand, we can interpret the Rossby numbers as if they would correspond to quite general rotation profiles $\Omega(R)$, which can have, e.g., the shape $\Omega(R) \sim R^w$ (with $w = -3/2$ and $\mathrm{Ro} = w/2 = -3/4$ for Kepler rotation).

In the following, we assume $\mathrm{Ro} \geqslant -1$ that corresponds to the centrifugally (Rayleigh) stable flow in the absence of the magnetic field. This reduces the conditions (37) to $\hat{a}_4 > 0$ that is equivalent to

$$\mathrm{Ro} > \mathrm{Ro}^c = -\frac{(1 + \mathrm{Ha}^{*2})^2 + 4\mathrm{Re}^{*2}}{4\mathrm{Re}^{*2}(\mathrm{PmHa}^{*2} + 1)}. \tag{39}$$

Note that in the absence of the magnetic field, $\mathrm{Ha}^* = 0$, the inequality (Equation (39)) is

$$\mathrm{Ro} > \mathrm{Ro}^v = -1 - \frac{1}{4\mathrm{Re}^{*2}}, \tag{40}$$

where we define the viscous Rayleigh line Ro^v. In the inviscid limit, $\mathrm{Re}^* \to \infty$ it is reduced to Rayleigh's centrifugal stability criterion:

$$\mathrm{Ro} > \mathrm{Ro}^i = -1, \tag{41}$$

where Ro^i is the classical inviscid Rayleigh line.

As is seen in the Figure 2(a), there are two extrema of the function $\mathrm{Ro}^c(\mathrm{Ha}^*)$ at

$$\mathrm{Ha}^*_{\max} = \pm\sqrt{\frac{-1 + \sqrt{(1 - \mathrm{Pm})^2 + 4\mathrm{Pm}^2\mathrm{Re}^{*2}}}{\mathrm{Pm}}}, \tag{42}$$

which agrees with the results of Ji et al. (2001). Triggered by the vertical magnetic field ($B_z^0 \neq 0$) at some values of Ha^* the flow becomes unstable for $\mathrm{Ro} > -1$. It can be stabilized again, however, with the further increase of Ha^*, which is a hallmark of the standard MRI, cf. with Figure 1 in Ji et al. (2001).

The maximal values of the Rossby number at the peaks of the boundary of the SMRI domain are

$$\mathrm{Ro}^c_{\max} = -\frac{4\mathrm{Re}^{*2}\mathrm{Pm}^2 + \left(\mathrm{Pm} - 1 + \sqrt{(1-\mathrm{Pm})^2 + 4\mathrm{Re}^{*2}\mathrm{Pm}^2}\right)^2}{4\mathrm{Re}^{*2}\mathrm{Pm}^2\sqrt{(1-\mathrm{Pm})^2 + 4\mathrm{Re}^{*2}\mathrm{Pm}^2}}. \tag{43}$$

The two extrema at $\mathrm{Ha}^*_{\max} \neq 0$ exist when the radicand in Equation (42) is positive, that is when

$$\mathrm{Re}^*\mathrm{Pm} > \frac{\sqrt{(2 - \mathrm{Pm})\mathrm{Pm}}}{2}. \tag{44}$$

Otherwise, the unique maximum is at the origin, Figure 2(b). This condition also follows from the positiveness of the second-order coefficient in the series expansion of $\mathrm{Ro}^c(\mathrm{Ha}^*)$ at $\mathrm{Ha}^* = 0$:

$$\mathrm{Ro}^c = -\frac{1 + 4\mathrm{Re}^{*2}}{4\mathrm{Re}^{*2}} - \frac{2 - (4\mathrm{Re}^{*2} + 1)\mathrm{Pm}}{4\mathrm{Re}^{*2}}\mathrm{Ha}^{*2} + \cdots. \tag{45}$$

Setting $\mathrm{Ro}^c_{\max} \geqslant -3/4$, we find the conditions for existence of the standard MRI at and above the Kepler line in terms of the magnetic Reynolds number $\mathrm{Rm}^* = \mathrm{Re}^*\mathrm{Pm}$:

$$\mathrm{Rm}^* \geqslant \frac{2}{3}\sqrt{1 + 3\mathrm{Pm}}. \tag{46}$$

For $\mathrm{Pm} \ll 1$ one should have $\mathrm{Rm}^* \geqslant 2/3$ to obtain SMRI for the Kepler flow, which leads to $\mathrm{Re}^* \gg 1$. At such values of Re^*, the following formal asymptotic expansions of $\mathrm{Ha}^*{}_{\max}(\mathrm{Re}^*)$ and $\mathrm{Ro}^c_{\max}(\mathrm{Re}^*)$ are valid:

$$\begin{aligned} \mathrm{Ha}^*{}_{\max} &= \pm\sqrt{2\mathrm{Re}^*} \mp \frac{\sqrt{2}}{4\mathrm{Pm}\sqrt{\mathrm{Re}^*}}, \\ \mathrm{Ro}^c_{\max} &= -\frac{1}{\mathrm{PmRe}^*} + \frac{1 - \mathrm{Pm}}{2\mathrm{Pm}^2\mathrm{Re}^{*2}} - \frac{(1 - \mathrm{Pm})^2}{2^3\mathrm{Pm}^3\mathrm{Re}^{*3}}. \end{aligned} \tag{47}$$

The asymptotic expansion (Equation (47)) gives a simple scaling law which is known to be a characteristic of SMRI:

$$\mathrm{Re}^* = \frac{1}{2}\mathrm{Ha}^{*2}. \tag{48}$$

This equation is identical to $N^* := \mathrm{Ha}^{*2}/\mathrm{Re}^* = 2$ where N^* is called interaction parameter (ratio of magnetic versus inertial effects, often used in technical magnetohydrodynamics) or Elsasser number (ratio of magnetic versus Coriolis effects, often used in geophysics and astrophysics).

The SMRI can be interpreted as destabilization of slow MC waves (Nornberg 2008; Nornberg et al. 2010). Indeed in the presence of shear, $\mathrm{Ro} \neq 0$, we find from Equation (32) with the

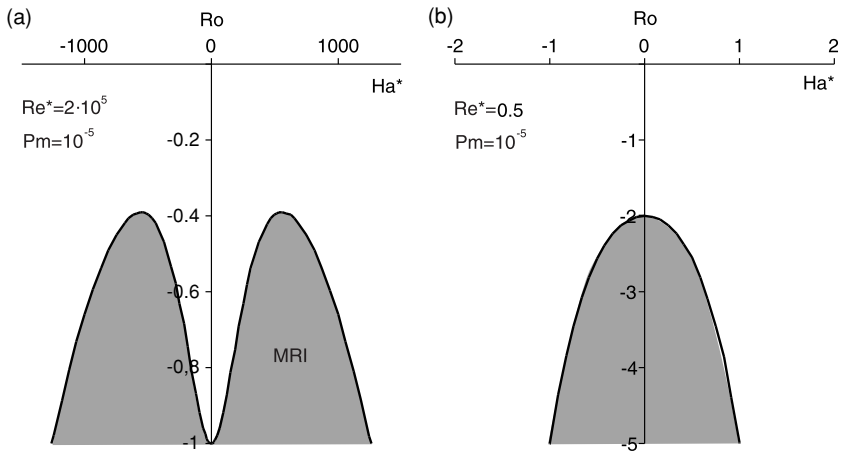

Figure 2. Domain according to Equation (39) of the standard MRI (gray) for $\mathrm{Pm} = 10^{-5}$ and (left) $\mathrm{Re}^* = 2 \times 10^5$ or (right) $\mathrm{Re}^* = 0.5$. The left plot shows the typical SMRI peaks (Ji et al. 2001).

coefficients (Equation (33)) that in the absence of dissipation ($\omega_\nu = 0$, $\omega_\eta = 0$) the eigenvalues are

$$\gamma = \pm\sqrt{-2\Omega_0^2\alpha^2(1+\mathrm{Ro}) - \omega_A^2 \pm 2\Omega_0\alpha\sqrt{\Omega_0^2\alpha^2(1+\mathrm{Ro})^2 + \omega_A^2}}. \tag{49}$$

At the critical value $\Omega_0 = \Omega_0^c$, where

$$\Omega_0^c = -\frac{\omega_A^2}{2\alpha^2 R_0 \partial_R \Omega}, \tag{50}$$

the branches of the slow magnetic–Coriolis waves merge with the origination of the double zero eigenvalue, see Figure 1(b). Splitting of this eigenvalue yields positive real eigenvalues, see Figure 1(c). Note that the SMRI threshold (Equation (50)) is equivalent to

$$\mathrm{Ro} = -\frac{\mathrm{Ha}^{*2}}{4\mathrm{Re}^{*2}\mathrm{Pm}} \tag{51}$$

that follows from Equation (39) when $\mathrm{Ha}^* \to \infty$.

4. HMRI IN THE PRESENCE OF AN AZIMUTHAL MAGNETIC FIELD ($\beta^* \neq 0$)

The fact that an additional azimuthal field changes the character of the MRI drastically had been detected by Knobloch as early as 1992 (Knobloch 1992). He had shown that in this case the instability appears in form of a traveling wave (see also Knobloch 1996). However, the difference in the scaling behavior for small Pm between standard and helical MRI was worked out only recently (Hollerbach & Rüdiger 2005), and is still the subject of intense debate. In this section, we will contribute to this discussion by focusing on the specific Pm dependence of the helical MRI.

4.1. Bilharz Criterion for Asymptotic Stability

With the appearance of the azimuthal magnetic field ($\beta^* \neq 0$), the coefficients of the polynomial $P(\lambda)$ become complex. This breaks the symmetry of the eigenvalues with respect to the real axis of the complex plane and consequently may lead to dramatic changes in the stability properties of the system.

In contrast to previous studies (Lakhin & Velikhov 2007; Rüdiger & Schultz 2008) that were based on the study of approximations to the roots of the dispersion relation

$$P(\lambda) = \lambda^4 + a_1\lambda^3 + a_2\lambda^2 + (a_3 + ib_3)\lambda + a_4 + ib_4 = 0, \tag{52}$$

we prefer to use the Bilharz criterion (Bilharz 1944; Marden 1966) of asymptotic stability of the roots of complex polynomials. This criterion establishes the necessary and sufficient conditions for all the roots to be in the left part of the complex plane ($\mathrm{Re}\lambda < 0$) in terms of positiveness of the main even-ordered minors of the Bilharz matrix. For the polynomial $P(\lambda)$ with the coefficients (Equation (35)) this matrix is

$$B = \begin{pmatrix} a_4 & -b_4 & 0 & 0 & 0 & 0 & 0 & 0 \\ b_3 & a_3 & a_4 & -b_4 & 0 & 0 & 0 & 0 \\ -a_2 & 0 & b_3 & a_3 & a_4 & -b_4 & 0 & 0 \\ 0 & -a_1 & -a_2 & 0 & b_3 & a_3 & a_4 & -b_4 \\ 1 & 0 & 0 & -a_1 & -a_2 & 0 & b_3 & a_3 \\ 0 & 0 & 1 & 0 & 0 & -a_1 & -a_2 & 0 \\ 0 & 0 & 0 & 0 & 1 & 0 & 0 & -a_1 \\ 0 & 0 & 0 & 0 & 0 & 0 & 1 & 0 \end{pmatrix}. \tag{53}$$

The Bilharz stability conditions (Bilharz 1944; Marden 1966) require positiveness of all diagonal even-ordered minors of B:

$$\begin{aligned} m_1 &= a_3a_4 + b_3b_4 > 0, \\ m_2 &= (a_2a_3 - a_1a_4)m_1 - a_2^2b_4^2 > 0, \\ m_3 &= (a_1a_2 - a_3)m_2 - \left(a_1^2a_4a_2 + (a_1b_3 - b_4)^2\right)m_1 \\ &\quad + a_1a_4\left(b_4a_2(2b_4 - a_1b_3) + a_1^2a_4^2\right) > 0, \\ m_4 &= a_1m_3 - a_1a_3m_2 + \left(a_3^3 + a_1^2b_4b_3 - 2a_1b_4^2\right)m_1 \\ &\quad + a_1b_4^2a_4(a_1a_2 - a_3) - b_4^2a_3^2a_2 + b_4^4 > 0. \end{aligned} \tag{54}$$

The inequalities (Equation (54)) determine the stability condition of the general dispersion relation (Equation (52)) in the presence of both vertical (B_z^0) and azimuthal (B_ϕ^0) components of the magnetic field.

We first note that for $\beta^* = 0$ the stability conditions (Equation (54)) are reduced to the stability condition $\hat{a}_4 > 0$ that was derived in the previous section. Indeed, with $\beta^* = 0$ the coefficients b_3 and b_4 vanish to zero, which yields

$$\begin{aligned} m_1 &= \hat{a}_4\hat{a}_3, \quad m_2 = \hat{a}_4\hat{a}_3(\hat{a}_2\hat{a}_3 - \hat{a}_1\hat{a}_4), \\ m_3 &= \hat{a}_4(\hat{a}_2\hat{a}_3 - \hat{a}_1\hat{a}_4)h_3, \quad m_4 = \hat{a}_4h_3^2. \end{aligned} \tag{55}$$

In view of $\hat{a}_3 > 0$ and $h_3 > 0$ it remains to check the sign of the expression $\hat{a}_2\hat{a}_3 - \hat{a}_1\hat{a}_4$. Explicit calculation yields

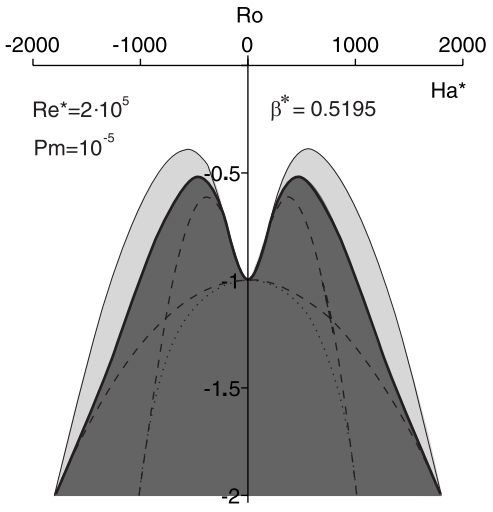

Figure 3. Domain according to Equation (39) of SMRI (light gray, $\beta^* = 0$) and that of HMRI (dark gray) for $\mathrm{Pm} = 10^{-5}$ and $\mathrm{Re}^* = 2 \times 10^5$. The thin full line marks the stability boundary $\mathrm{Ro} = \mathrm{Ro}^c$. The dashed, dotted, and bold lines bound the domains where the Bilharz minors $m_{1,2,3,4} > 0$. The domain of HMRI which is adjacent to the intersection of these domains is shown in dark gray. The boundary to the HMRI domain (bold line) is $m_4 = 0$.

$$\frac{\hat{a}_2\hat{a}_3 - \hat{a}_1\hat{a}_4}{2} = \frac{(4\mathrm{PmRe}^{*2}(\mathrm{Ro}+1) + \mathrm{Pm} + \mathrm{Ha}^{*2} + 2)^2\mathrm{Pm}}{\mathrm{Pm}\sqrt{\mathrm{Pm}}} + \frac{(4\mathrm{Re}^{*2}\mathrm{Pm}^2+1)(\mathrm{Pm}+1)\mathrm{Ha}^{*2}+\mathrm{Pm}^2\mathrm{Ha}^{*2}(\mathrm{Ha}^{*2}+3+\mathrm{Pm})+1}{\mathrm{Pm}\sqrt{\mathrm{Pm}}} > 0. \tag{56}$$

Therefore, for $\beta^* = 0$ the conditions (Equation (55)) are reduced to the inequality $\hat{a}_4 > 0$ that determines the stability domain that is adjacent to the domain of SMRI.

In Figure 3, we plot the boundary (Equation (39)) of the SMRI domain to compare it with the domain of HMRI given by the inequalities (Equation (54)). We see that the domain $m_4 > 0$ is an intersection of all the domains $m_i > 0$, $i = 1, 2, 3, 4$. Thus, the region of HMRI, shown by dark gray in Figure 3, is adjacent to the domain $m_4 > 0$. Although this fact is not a proof that the inequalities (Equation (54)) are reduced to the last one, our numerical computations of the domains and of the roots of the dispersion relation as well as the analysis of the inductionless approximation in the next section confirm that $m_4 = 0$ is the boundary of HMRI domain.

4.2. Inductionless Approximation

As it was first observed in Priede et al. (2007), a remarkable feature of HMRI is that it leads to destabilization, even in the limit $\mathrm{Pm} \to 0$, for some $\mathrm{Ro} > -1$, although not until the Kepler profile ($\mathrm{Ro} = -0.75$). Below we prove this.

Let us consider the Rossby number as a function of the magnetic Prandtl number and fix all other parameters. Substituting $\mathrm{Ro} = a + b\mathrm{Pm} + \cdots$ into the equation $m_4 = 0$ and collecting the terms with the identical powers of Pm, we find a quadratic equation in the coefficient a, which can be exactly solved. Therefore, in the limit $\mathrm{Pm} \to +0$ there are two branches of the function $\mathrm{Ro}(\mathrm{Ha}^*, \mathrm{Re}^*, \beta^*)$: a positive one ($\mathrm{Ro}^+ > 0$) and a negative one ($\mathrm{Ro}^- < 0$),

$$\mathrm{Ro}^{\pm} = \frac{\left(1+\mathrm{Ha}^{*2}\right)^2+4\beta^{*2}\mathrm{Ha}^{*2}(1+\beta^{*2}\mathrm{Ha}^{*2})}{2\beta^{*2}\mathrm{Ha}^{*4}} \pm \frac{(2\beta^{*2}\mathrm{Ha}^{*2}+\mathrm{Ha}^{*2}+1)\sqrt{\left(1+\mathrm{Ha}^{*2}\right)^2+4\beta^{*2}\mathrm{Ha}^{*2}(1+\beta^{*2}\mathrm{Ha}^{*2})+\frac{\mathrm{Ha}^{*4}\beta^{*2}}{\mathrm{Re}^{*2}}\left(\left(1+\mathrm{Ha}^{*2}\right)^2+4\beta^{*2}\mathrm{Ha}^{*2}\right)}}{2\mathrm{Ha}^{*4}\beta^{*2}}. \tag{57}$$

When $\beta^* \to +0$ the function Ro^+ tends to infinity while for Ro^- we get

$$\lim_{\beta^* \to +0} \mathrm{Ro}^- = -1 - \frac{\left(1+\mathrm{Ha}^{*2}\right)^2}{4\mathrm{Re}^{*2}}. \tag{58}$$

The expression (58) can also be obtained as a limit of Ro^c defined in Equation (39) when $\mathrm{Pm} \to +0$.

Calculating the derivative $\frac{\partial \mathrm{Ro}^-}{\partial \mathrm{Re}^*}$, we find that it is strictly positive for all $\mathrm{Re}^* \in (0, +\infty)$,

$$\frac{\partial \mathrm{Ro}^-}{\partial \mathrm{Re}^*} = \frac{(1+\mathrm{Ha}^{*2})^3+\beta^{*2}\mathrm{Ha}^{*2}(6+8\mathrm{Ha}^{*2}+2\mathrm{Ha}^{*4}+8\beta^{*2}\mathrm{Ha}^{*2})}{2\mathrm{Re}^{*2}\sqrt{\mathrm{Re}^{*2}((1+\mathrm{Ha}^{*2})^2+4\beta^{*2}\mathrm{Ha}^{*2}(1+\beta^{*2}\mathrm{Ha}^{*2}))+\mathrm{Ha}^{*4}\beta^{*2}((1+\mathrm{Ha}^{*2})^2+4\beta^{*2}\mathrm{Ha}^{*2})}} > 0. \tag{59}$$

Consequently, the maximal value of $\mathrm{Ro}^- < 0$ is attained when $\mathrm{Re}^* \to +\infty$. In this limit, the function $\mathrm{Ro}^-(\beta^*)$ has a maximum

$$\mathrm{Ro}^-_{\max}(\mathrm{Ha}^*) = \max_{\beta^*} \lim_{\mathrm{Re}^* \to +\infty} \mathrm{Ro}^- = -\frac{-\mathrm{Ha}^{*2} - 2 + \sqrt{4 + 6\mathrm{Ha}^{*2} + 2\mathrm{Ha}^{*4}}}{2\mathrm{Ha}^{*2}} \tag{60}$$

at

$$\beta^*_{\max}(\mathrm{Ha}^*) = \frac{\sqrt{2 + 2\mathrm{Ha}^{*2}}}{2\mathrm{Ha}^*}. \tag{61}$$

Since the derivative of the function $\mathrm{Ro}^-_{\max}(\mathrm{Ha}^*)$ is strictly positive for all $\mathrm{Ha}^* > 0$,

$$\frac{d\mathrm{Ro}^-_{\max}(\mathrm{Ha}^*)}{d\mathrm{Ha}^*} = 4\frac{3\mathrm{Ha}^{*2} + 4 - 2\sqrt{4 + 6\mathrm{Ha}^{*2} + 2\mathrm{Ha}^{*4}}}{\mathrm{Ha}^{*3}\sqrt{4 + 6\mathrm{Ha}^{*2} + 2\mathrm{Ha}^{*4}}} > 0, \tag{62}$$

we conclude that the global maximum of the function $\mathrm{Ro}^-(\mathrm{Ha}^*, \mathrm{Re}^*, \beta^*)$ coincides with the maximal value of $\mathrm{Ro}^-_{\max}(\mathrm{Ha}^*)$, which is attained at $\mathrm{Ha}^* \to +\infty$ and is therefore

$$\max_{\mathrm{Ha}^*, \mathrm{Re}^*, \beta^*} \mathrm{Ro}^- = \max_{\mathrm{Ha}^*} \mathrm{Ro}^-_{\max}(\mathrm{Ha}^*) = 2 - 2\sqrt{2} \simeq -0.8284, \tag{63}$$

being exactly the same value that was found in the highly resistive inviscid limit in Liu et al. (2006). The corresponding optimal value of β^* in the limit $\mathrm{Ha}^* \to +\infty$ is

$$\beta^*_{\max} = \frac{\sqrt{2}}{2} \simeq 0.7071. \tag{64}$$

Note that numerical maximization of Ro frequently leads to the extrema corresponding to the values of $\beta^* \simeq 0.7$ even for $\mathrm{Pm} \neq 0$.

Extending the inviscid result of Liu et al. (2006), we establish that in the inductionless approximation ($\mathrm{Pm} = 0$) the upper bound for HMRI is

$$\mathrm{Ro}^-(\mathrm{Ha}^*, \mathrm{Re}^*, \beta^*) < 2 - 2\sqrt{2} \simeq -0.8284. \tag{65}$$

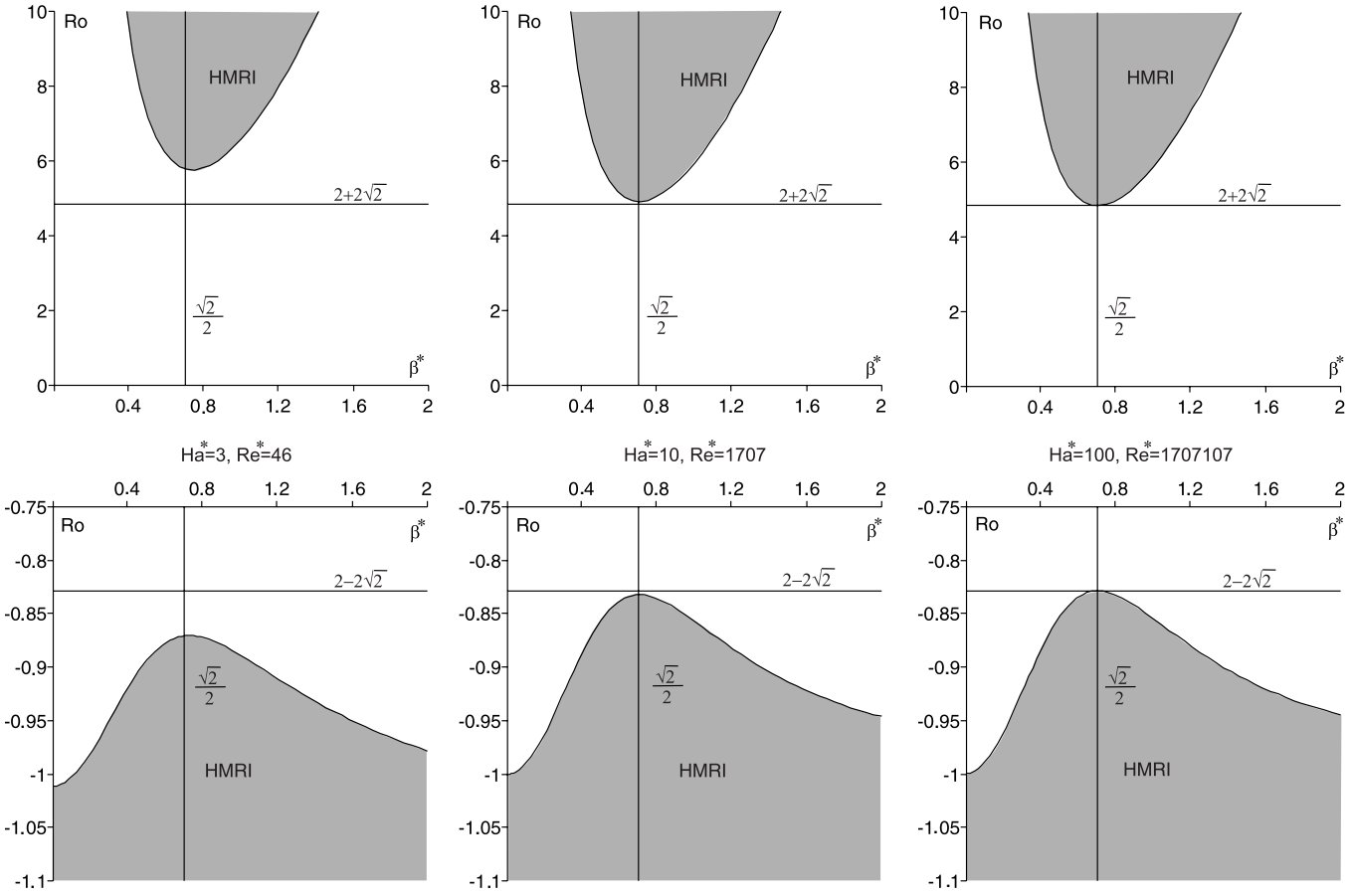

Figure 4. Inductionless approximation (Pm = 0): two domains (Equation (57)) of HMRI (gray) are within the bounds (Equation (67)). It is seen how the scaling law (Equation (68)) works. HMRI is possible even for Pm = 0—the paradox of inductionless magnetorotational instability (Priede et al. 2007).

Proceeding similarly, we find that

$$\mathrm{Ro}^{+}(\mathrm{Ha}^{*}, \mathrm{Re}^{*}, \beta^{*}) > 2 + \sqrt{2} \simeq 4.8284, \tag{66}$$

where the minimum is attained at the same extremal value of β^{*} given by Equation (64). The lower bound (Equation (66)) for Ro^{+} exactly coincides with that found in Liu et al. (2006) in the highly resistive inviscid limit by analyzing the roots of the dispersion relation. However, it should be noticed that the character of this Ro^{+} is still unclear. Since up to present we have not obtained any corresponding result from a one-dimensional global eigenvalue solver, it remains to be checked if this result is an artefact of the short wavelength approximation.

Anyway, quite in accordance with Lakhin & Velikhov (2007) and Liu et al. (2007), we conclude that in the inductionless approximation there is no HMRI for

$$2 - 2\sqrt{2} < \mathrm{Ro}(\mathrm{Ha}^{*}, \mathrm{Re}^{*}, \beta^{*}) < 2 + 2\sqrt{2}, \tag{67}$$

which excludes HMRI for the Kepler law and for other shallower velocity profiles.

Finally, we would like to find a scaling law for HMRI to compare it with that of SMRI (Equation (48)). The HMRI scaling law for the maximum of the critical Rossby number at infinity (which works well, however, starting from $\mathrm{Ha}^{*} \simeq 3$) reads

$$\mathrm{Re}^{*} = \left(1 + \frac{\sqrt{2}}{2}\right)\mathrm{Ha}^{*3}. \tag{68}$$

In terms of the interaction parameter, this can be rewritten as $N^{*}\mathrm{Ha}^{*} = 1/(1 + \sqrt{2}/2)$. This scaling is rather different from the scaling of SMRI (Equation (45)).

In Figure 4, the two domains (Equation (57)) of HMRI in the inductionless approximation (Pm = 0) are plotted for the Hartmann and Reynolds numbers that change according to the scaling law (Equation (68)). It is seen that the helical MRI regions are within the bounds (Equation (67)) which are reached only at $\beta^{*} = \sqrt{2}/2$.

4.3. HMRI in the Case when Pm ≠ 0

In the previous section, we have confirmed that for Pm = 0, HMRI does not work for Keplerian flows, at least according to the WKB approximation. Nevertheless, Hollerbach and Rüdiger had shown that it does when considered as an eigenvalue problem, provided that at least one radial boundary is conducting (Rüdiger & Hollerbach 2007).

In this section, we analyze the dispersion relation without the simplifying assumption that Pm = 0. As it follows from Equation (39), in the absence of the azimuthal component of the magnetic field ($\beta^{*} = 0$) there is no SMRI for $\mathrm{Pm} < \mathrm{Pm}^{c}$, where at the threshold

$$\mathrm{Pm} = \mathrm{Pm}^{c} := -\frac{\left(1 + \mathrm{Ha}^{*2}\right)^{2} + 4\mathrm{Re}^{*2}(1 + \mathrm{Ro})}{4\mathrm{Ro}\mathrm{Re}^{*2}\mathrm{Ha}^{*2}}. \tag{69}$$

The SMRI in this case develops when $\mathrm{Pm} > \mathrm{Pm}^{c}$. In Figure 5, the threshold (Equation (69)) is shown by the dashed line.

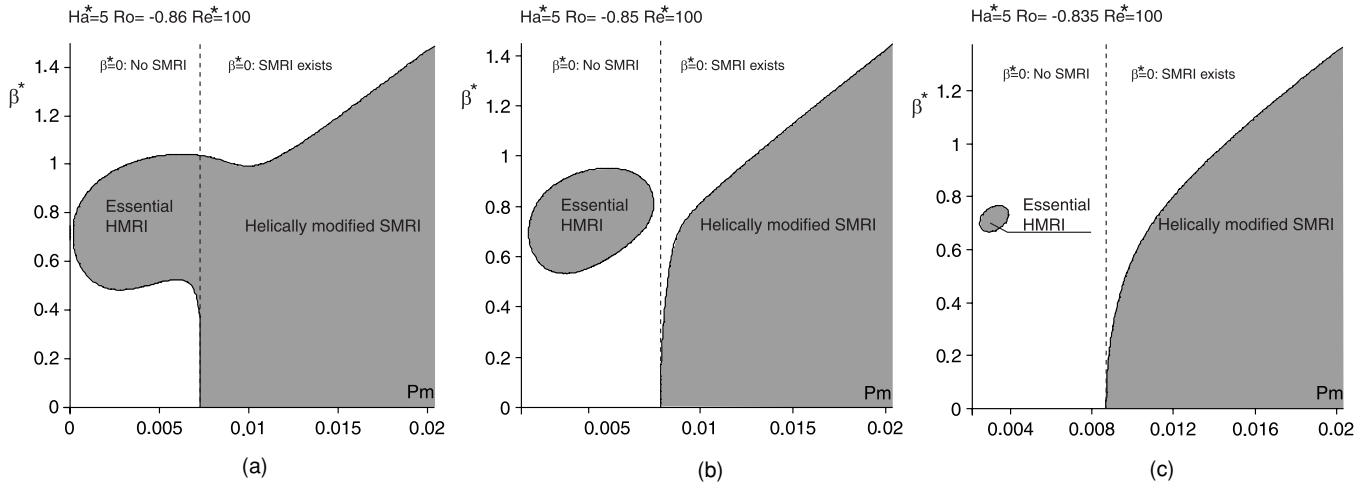

Figure 5. Relation of SMRI (right to the dashed line for $\beta^* = 0$) and HMRI (gray area). For $\beta^* \neq 0$ a (semi)-island of the essential HMRI exists in the neighborhood of $\beta^* = \sqrt{2}/2$ for the values of Pm at which SMRI was not possible in the absence of the azimuthal magnetic field ($\beta^* = 0$). The size of the essential HMRI island decreases with the increase of Ro.

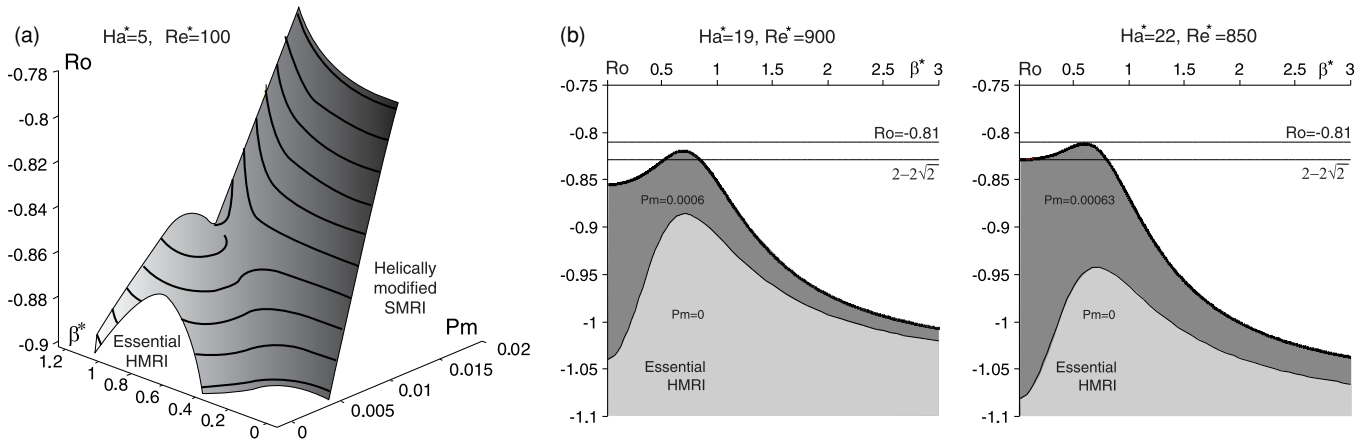

Figure 6. (a) Boundary of the three-dimensional HMRI domain in the (Pm, β^*, Ro)-space with the local maximum over the area of the essential HMRI in the (Pm, β^*)-plane and (b) for $\mathrm{Pm} \neq 0$ the essential HMRI domain can exceed the bound $\mathrm{Ro} = 2 - 2\sqrt{2}$ that is valid in the inductionless case ($\mathrm{Pm} = 0$). Thin lines show the boundary of the essential HMRI domain in the inductionless approximation (light gray), bold ones—the boundary of the essential HMRI domain in the case when $\mathrm{Pm} \neq 0$ (dark gray).

4.3.1. First Scenario of HMRI Excitation

When the azimuthal magnetic field is switched on ($\beta^* \neq 0$), the instability threshold Pm^c depends on β^*. At small values of β^*, the threshold slightly increases so that the boundary of the domain of instability bends to the right of the dashed line in the (Pm, β^*)-plane (see Figure 5). The behavior of the instability boundary with further increase of β^* is determined by the Rossby number.

For Rossby numbers close to $\mathrm{Ro} = -1$, the instability boundary at some $\beta^* \neq 0$ bends to the left, crosses the dashed line and forms a "semi-island" of instability with its center located close to $\beta^* = \frac{\sqrt{2}}{2}$, Figure 5(a). This enlargement of the instability domain on the left of the dashed line relies on a sort of optimal helicity of the applied magnetic field because neither at smaller nor at larger values of $\beta^* \neq 0$ there is any instability in this range of Pm. Although the whole gray area of instability in Figure 5(a) is of course the region of the HMRI, the main interesting effect of non-zero helicity is the excitation of instability at small and even infinitesimally small values of Pm in the range where SMRI is not possible. With the increase of Ro the specific effect of β^* becomes even more pronounced with the bifurcation of the instability domain to the isolated region (island) that lies on the left of the dashed line and to the "continent" on the right of it, Figures 5(b) and (c). The island of HMRI illustrates both the destabilizing role of the azimuthal magnetic field component and the non-triviality of inducing HMRI below the threshold (Equation (69)) at small negative values of the Rossby number ($\mathrm{Ro} > -1$). For these reasons, we propose to refer to the instability for $\beta^* \neq 0$ on the left of the dashed line as the *essential HMRI* and that on the right as the *helically modified SMRI*.

Despite the apparent discontinuities in the (β^*, Ro)-plane, the three-dimensional domain of HMRI in the (β^*, Pm, Ro)-space has a smooth boundary given by the expression $m_4 = 0$, Figure 6(a). As it is seen in Figure 6(a), the function $\mathrm{Ro}^c(\mathrm{Pm}, \beta^*)$ has local extrema at some $\mathrm{Pm} \neq 0$, yielding regions of HMRI that are separated from each other in the plane (Pm, β^*), Figures 5(b) and (c). Since the maximum is attained at small but finite values of Pm, the corresponding boundary of HMRI in the (β^*, Ro)-plane at $\mathrm{Pm} \neq 0$ can exceed that in the inductionless limit (an instability induced by the viscosity $\omega_\nu \neq 0$) and, moreover, the limiting bound $\mathrm{Ro} = 2 - 2\sqrt{2}$, as is clearly seen in Figure 6(b). The one-dimensional slices of

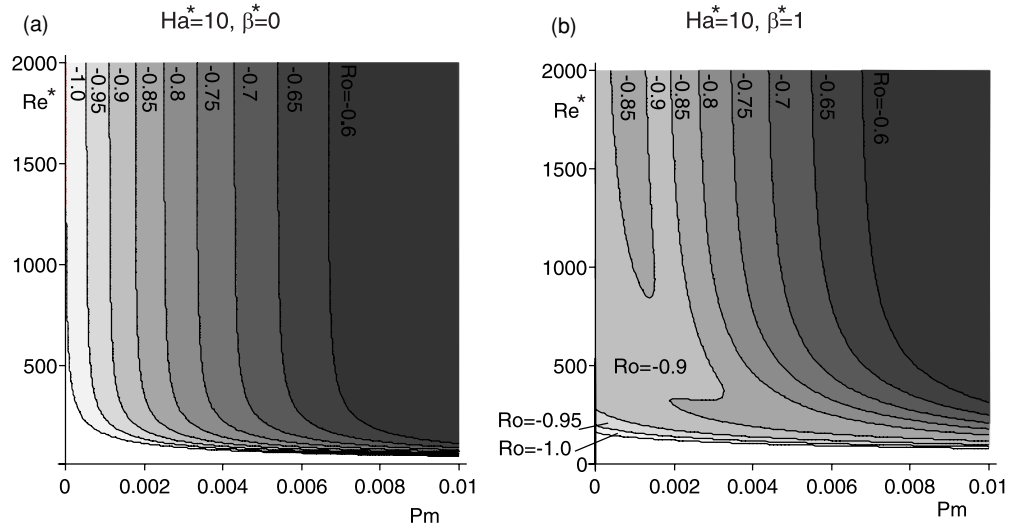

Figure 7. (a) SMRI domains shown in gray with the intensity of the color corresponding to various values of Ro and (b) a considerable deformation and even breaking of the instability domains in the region of small Pm when β^* is switched on (HMRI). The pictures are in agreement with the calculations of (Rüdiger & Schultz 2008).

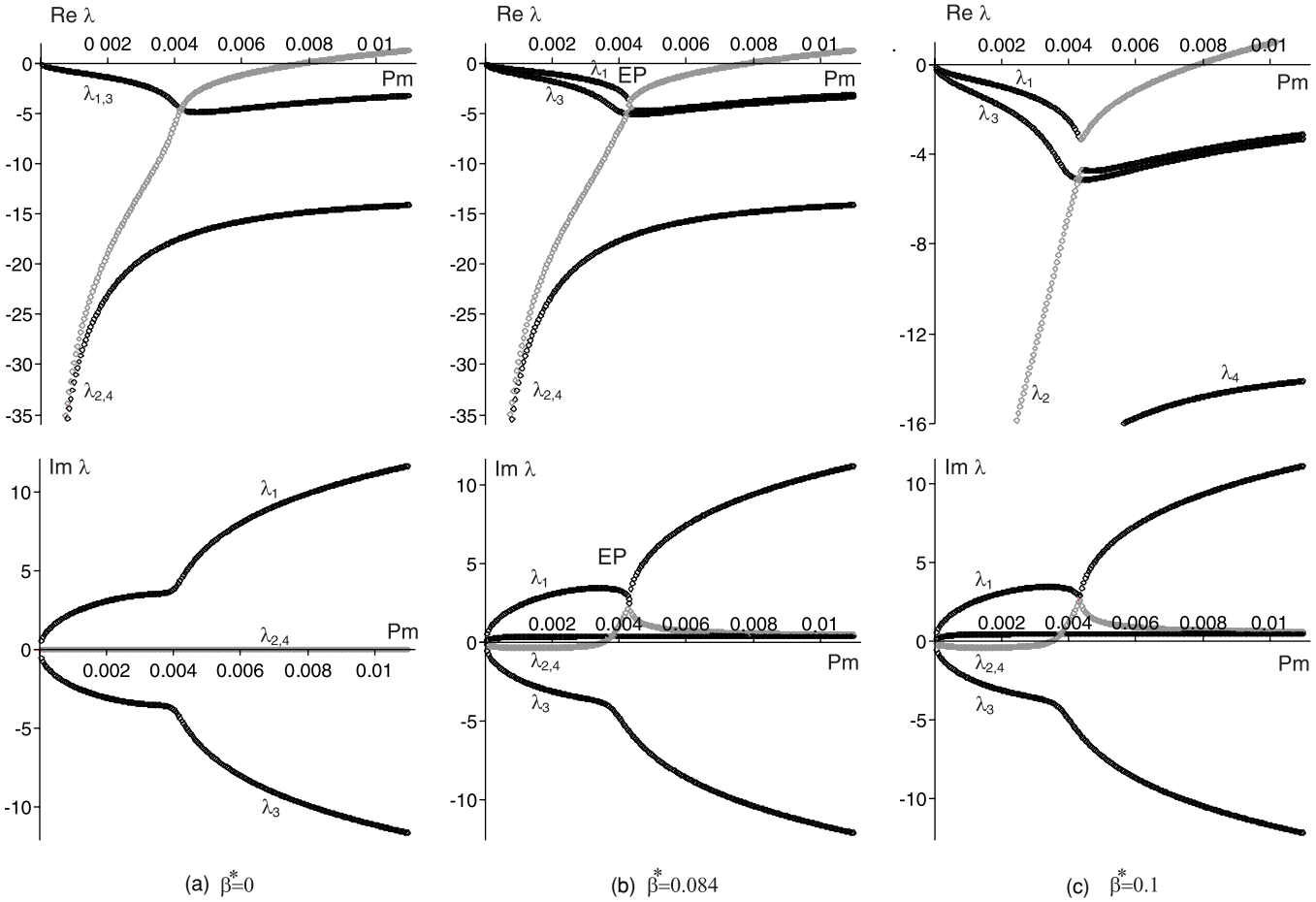

Figure 8. Ha* = 5, Re* = 100, and Ro = −0.85: real and imaginary parts of eigenvalues $\lambda_{1,2,3,4}$ as functions of Pm. (a) Two stable complex branches (inertial modes) with the coincident real parts and two pure real ones, one of the latter shown in gray becomes positive and yields SMRI; (b) merging of the inertial complex mode with the deformed unstable helically modified SMRI-branch (gray) with the origination of an exceptional point (EP); and (c) bifurcation yields new mixed complex eigenvalue branches thus creating new opportunities for instability at low Pm.

the three-dimensional instability domain in the (β^*, Ro)-plane converge, however, to the region of the inductionless HMRI when Pm → 0. Therefore, in comparison to the inductionless limit, for Pm ≠ 0 we obtain higher values of the maximal Rossby numbers corresponding to the excitation of HMRI—a quite promising similarity of this local WKB analysis with the observation of HMRI for Keplerian flows with conducting boundaries in Rüdiger & Hollerbach (2007). In Figure 7, the

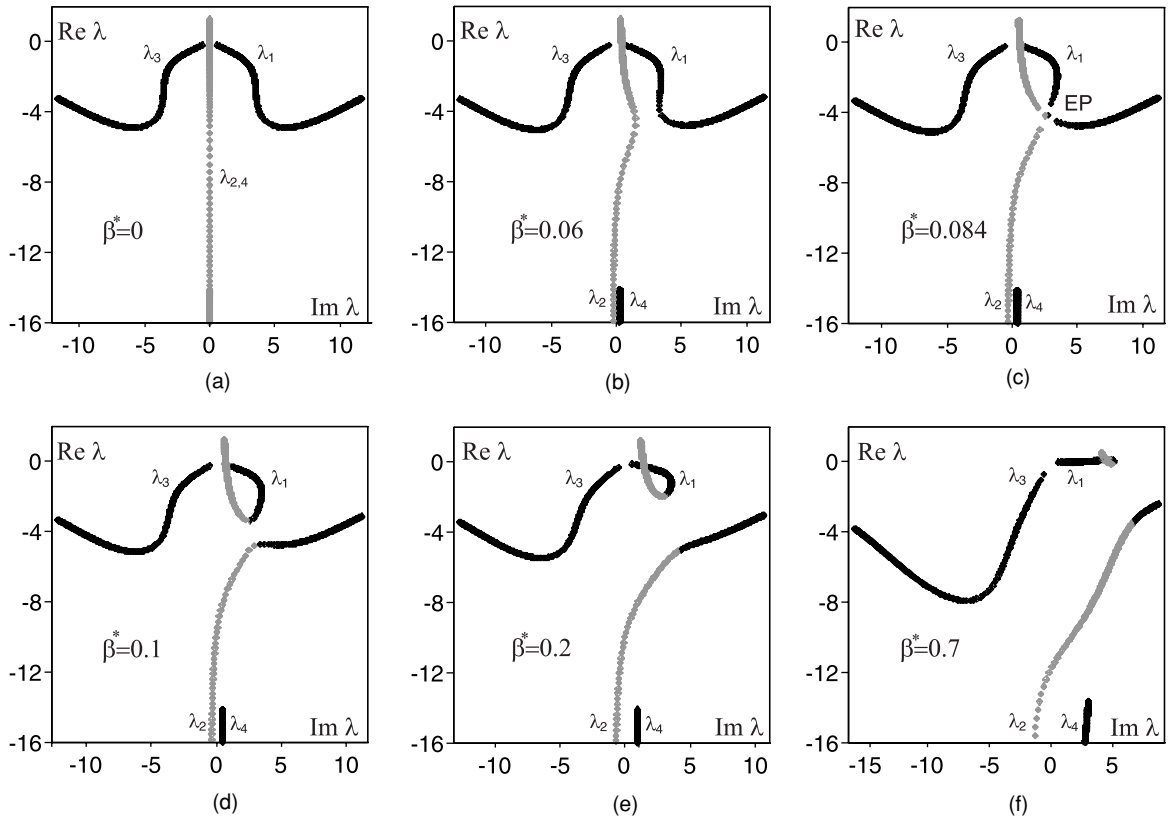

Figure 9. $\mathrm{Ha}^* = 5$, $\mathrm{Re}^* = 100$, and $\mathrm{Ro} = -0.85$: eigenvalue trajectories in the complex plane when Pm changes from zero to $\mathrm{Pm} = 0.011$ show the effect of transfer of instability between branches through a spectral exceptional point (EP). (a) SMRI is caused by the transition of a pure real eigenvalue from negative values to positive; (b) deformation of the critical branch (gray) for $\beta^* \neq 0$; (c) merging of the critical and stable branches with the origination of the double complex eigenvalue with the Jordan block—exceptional point (EP); ((d)–(f)) splitting of the EP and bifurcation of the eigenvalue trajectories: after a surgery the stable complex branch acquires an unstable tail of the critical branch (gray) and becomes unstable near the origin, which corresponds to an unstable traveling wave of HMRI.

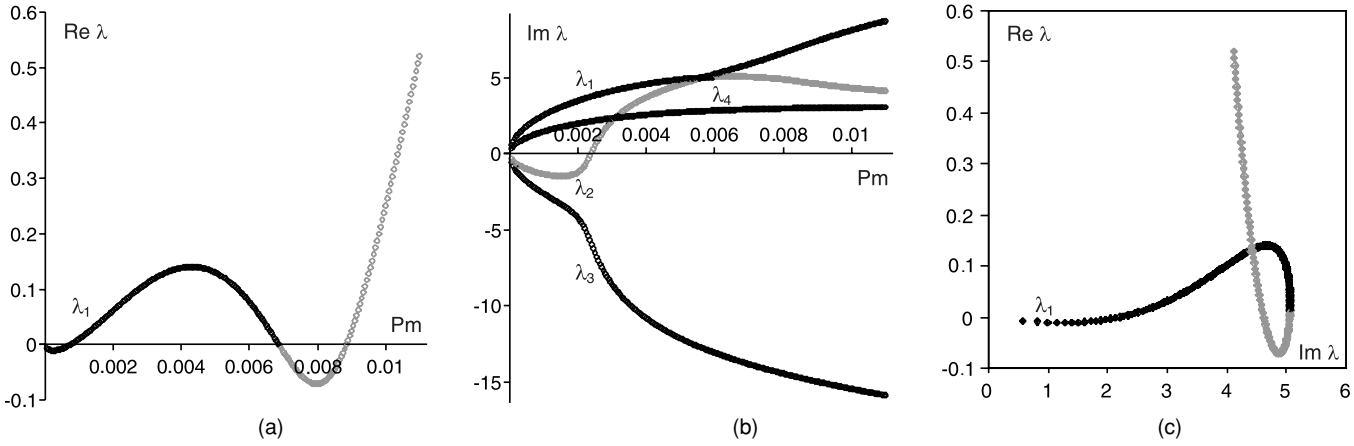

Figure 10. $\mathrm{Ha}^* = 5$, $\mathrm{Re}^* = 100$, and $\mathrm{Ro} = -0.85$, $\beta^* = 0.7$: (a) real part of the new critical eigenvalue branch, combined from the parts of λ_1 (black) and λ_2 (gray), is positive while Pm is within the island of the essential HMRI and the continent of the helically modified SMRI; (b) imaginary parts of the new stable and unstable branches; and (c) trajectory in the complex plane of the new critical eigenvalue that creates instability with the change of Pm from zero to $\mathrm{Pm} = 0.011$.

detailed evolution of the stability boundaries in the $(\mathrm{Pm}, \mathrm{Re}^*)$-plane with the increase of Ro for $\beta^* = 0$ and $\beta^* = 1$ demonstrates that the mechanism of reduction of the critical Reynolds number, which is another important characteristic of HMRI, is accompanied by a qualitative effect—a breakup of the instability domain into two disjoint regions.

To clarify the nature of HMRI and SMRI and their relation to each other, we inspect now the roots of the dispersion relation as functions of Pm. Series expansions of the roots in the vicinity of $\mathrm{Pm} = 0$ at $\beta^* = 0$ yield

$$\lambda_{1,3} = \left[-1 - \mathrm{Ha}^{*2} \pm 2\mathrm{Re}^* \sqrt{-(1+\mathrm{Ro})} \right] \sqrt{\mathrm{Pm}} + o(\mathrm{Pm}^{1/2}),$$
$$\lambda_{2,4} = -\frac{1}{\sqrt{\mathrm{Pm}}} + \mathrm{Ha}^{*2} \sqrt{\mathrm{Pm}} + o(\mathrm{Pm}^{1/2}). \quad (70)$$

Therefore, two eigenvalues $\lambda_{1,3}$ branch from zero and the other two $\lambda_{2,4}$ branch from minus infinity. The eigenvalues $\lambda_{2,4}$ are real and negative, whereas the eigenvalues $\lambda_{1,3}$ are real in the

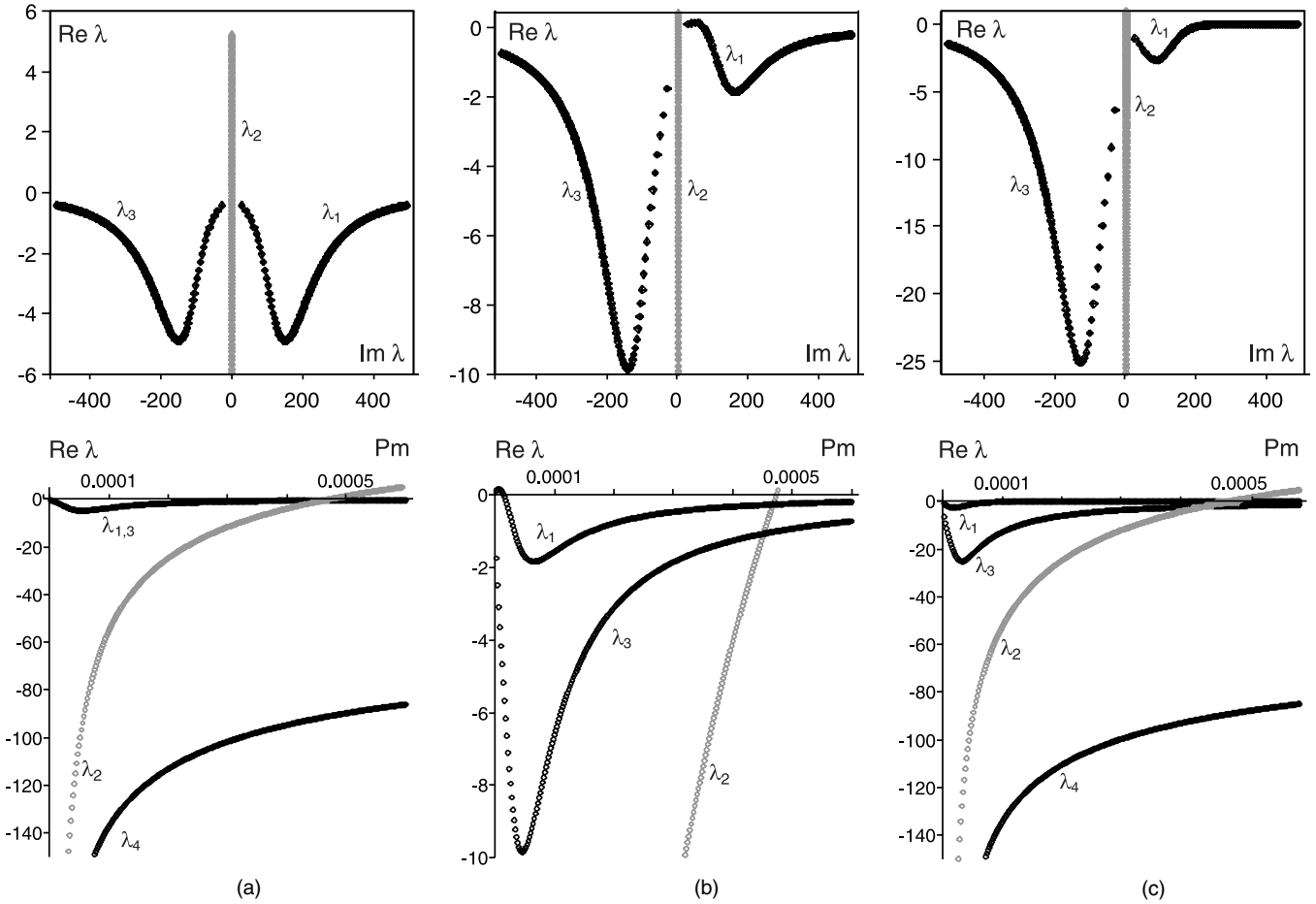

Figure 11. $\mathrm{Ha}^* = 17$, $\mathrm{Re}^* = 28850$, and $\mathrm{Ro} = -0.88$: (a) stable inertial waves ($\lambda_{1,3}$) and critical SMRI branch (in gray) of the real eigenvalues ($\lambda_{2,4}$) for $\beta^* = 0$; (b) for $\beta^* = 0.7$ one of the inertial wave branches becomes unstable independently of the SMRI branch; and (c) for $\beta^* = 2$ the same inertial wave branch becomes unstable a second time at higher frequencies independently of the SMRI branch.

vicinity of the origin for $\mathrm{Ro} \leqslant -1$ and complex otherwise with the frequency

$$\omega = 2\Omega_0 \frac{k_z}{k}\sqrt{\mathrm{Ro}+1}.$$

The eigenvalues $\lambda_{1,3}$ correspond to inertial waves with $\omega = \omega_C := 2\Omega_0 k_z/k$, if we assume rotation without shear ($\mathrm{Ro} = 0$) and without damping, see, e.g., Nornberg et al. (2010).

In the particular case, when $\beta^* = 0$ and $\mathrm{Ro} = -1$ the dispersion equation is exactly solved:

$$\lambda_{1,2} = \frac{-\mathrm{Pm}-1\pm\sqrt{(\mathrm{Pm}-1)^2-4\mathrm{Pm}\mathrm{Ha}^*(\mathrm{Ha}^*-2\sqrt{\mathrm{Pm}})\mathrm{Re}^*}}{2\sqrt{\mathrm{Pm}}},$$
$$\lambda_{3,4} = \frac{-\mathrm{Pm}-1\pm\sqrt{(\mathrm{Pm}-1)^2-4\mathrm{Pm}\mathrm{Ha}^*(\mathrm{Ha}^*+2\sqrt{\mathrm{Pm}})\mathrm{Re}^*}}{2\sqrt{\mathrm{Pm}}}. \quad (71)$$

The eigenvalues (Equation (71)) are real near the origin, because $\mathrm{Ro} = -1$:

$$\lambda_{1,3} = -\sqrt{\mathrm{Pm}} - \mathrm{Ha}^{*2}\sqrt{\mathrm{Pm}} \pm 2\mathrm{Re}^*\mathrm{Ha}^*\mathrm{Pm} + o(\mathrm{Pm}),$$
$$\lambda_{2,4} = -\frac{1}{\sqrt{\mathrm{Pm}}} + \mathrm{Ha}^{*2}\sqrt{\mathrm{Pm}} \mp 2\mathrm{Re}^*\mathrm{Ha}^*\mathrm{Pm} + o(\mathrm{Pm}). \quad (72)$$

Equating the roots $\lambda_{2,4}$ to zero, we reproduce the expression for the threshold (Equation (69)) at $\mathrm{Ro} = -1$.

In another particular case, when $\beta^* = 0$, $\mathrm{Re}^* = 0$, and $\mathrm{Ro} = 0$ the exact solution to the dispersion equation consists of two double eigenvalues

$$\lambda = -\frac{1}{2}\left(\sqrt{\mathrm{Pm}} + \frac{1}{\sqrt{\mathrm{Pm}}}\right) \pm \sqrt{\frac{1}{4}\left(\sqrt{\mathrm{Pm}} - \frac{1}{\sqrt{\mathrm{Pm}}}\right)^2 - \mathrm{Ha}^{*2}}$$

that are expressed in terms of the viscous, resistive, and Alfvén frequencies in Equation (30).

Consider the eigenvalues corresponding to the values of parameters of Figure 5. Since $\mathrm{Ro} = -0.85 > -1$, there are two real and two complex branches of eigenvalues $\lambda = \lambda(\mathrm{Pm})$ at $\beta^* = 0$. In the upper subfigure of Figure 8(a), the real parts of the two complex branches $\lambda_{1,3}$ coincide forming a single curve $\mathrm{Re}\lambda(\mathrm{Pm})$ with $\mathrm{Re}\lambda(0) = 0$. The branches of pure real eigenvalues $\lambda_{2,4}$ form two different curves of the real parts $\mathrm{Re}\lambda(\mathrm{Pm})$ and two identical curves of the imaginary parts $\mathrm{Im}\lambda(\mathrm{Pm}) \equiv 0$, Figure 8(a). One of the real branches $\lambda_{2,4}$ that comes from minus infinity changes its sign at the threshold (Equation (69)) and excites SMRI with zero eigenfrequency. Due to the large negative values of the real eigenvalues of the critical branch, there is no way to destabilize the flow at small Pm. However, new opportunities for destabilization occur with the increase of β^* that is accompanied by the qualitative change in the configuration of the eigenvalue branches.

When the azimuthal component of the magnetic field is switched on, the real eigenvalues of the critical branch (λ_2),

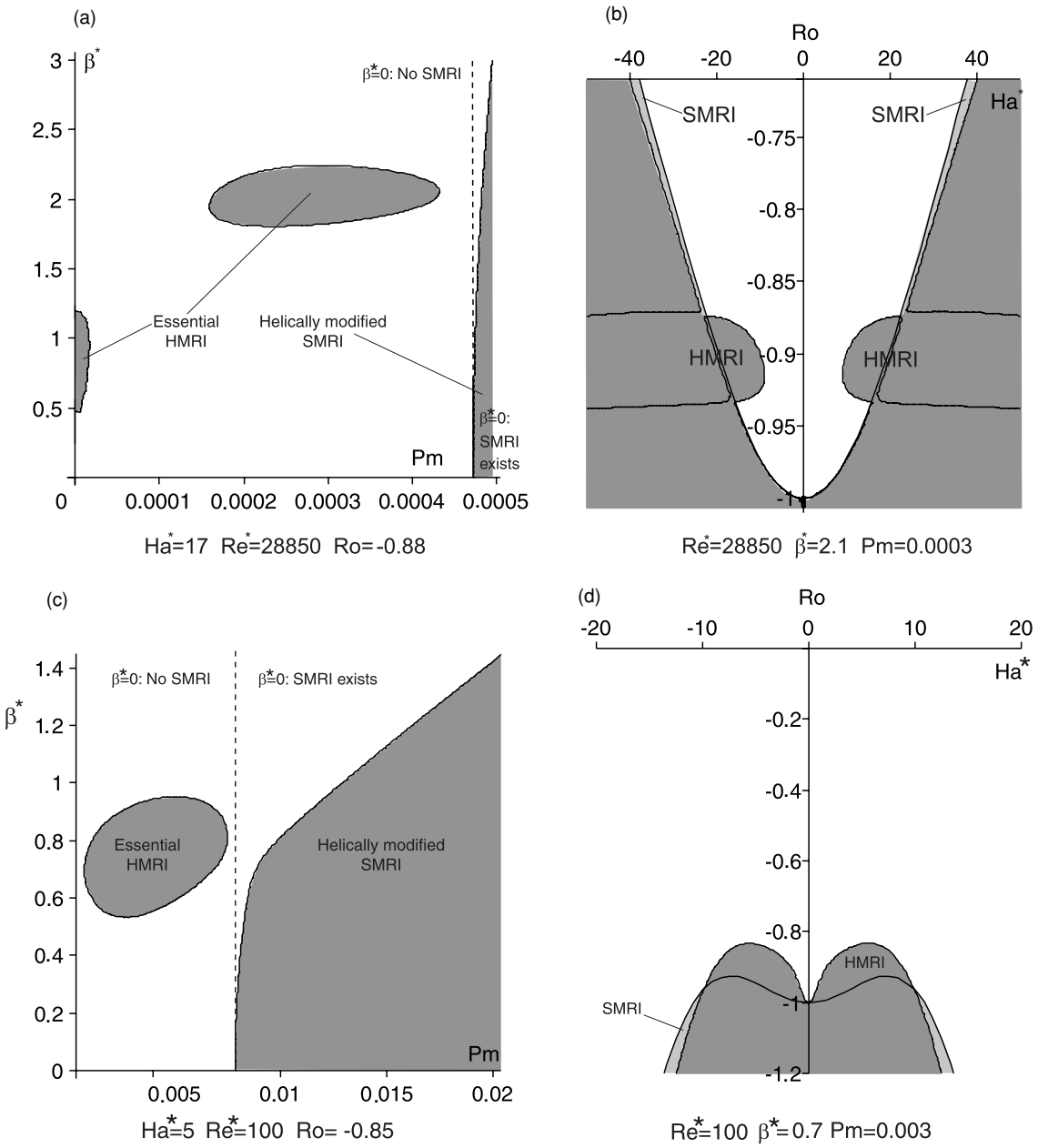

Figure 12. (a) First and second islands of the essential HMRI developed according to the second scenario in the neighborhood of $\beta^* = \sqrt{2}/2$ and $\beta^* = 3\sqrt{2}/2$, (b) an essential HMRI inclusion in the helically modified SMRI domain, (c) an island of the essential HMRI developed according to the first scenario, and (d) the corresponding view in the (Ha*, Ro)-plane.

shown in gray in Figure 8, get complex increments. Note that the perturbation splits the coincident curves of the real parts of the roots $\lambda_{1,3}$ into two different curves Reλ(Pm), see Figures 8(b) and (c). Similar splitting of the coincident curves of the imaginary parts of the roots $\lambda_{2,4}$ yields two different curves Imλ(Pm) in Figures 8(b) and (c). By this reason, the total number of the branches in Figures 8(b) and (c) increases up to four in comparison with the three ones that are visible in Figure 8(a).

With the increase of β^*, the critical real branch (λ_2) deforms and interacts with a stable complex one (λ_1) of an inertial wave until at $\beta^* \simeq 0.084$ they merge at a point with the origination of the double complex eigenvalue with the Jordan block known as an exceptional point (EP; Berry 2004; Mailybaev et al. 2005), see Figure 8(b). Notice that another EP corresponds to negative β^*. With the further increase of β^* this configuration bifurcates into a new one, where parts of the stable and unstable branches are interchanged (Figure 8(c)). The new critical eigenvalue branch consists of complex eigenvalues that demonstrate the typical generalized crossing scenario near an EP (Or 1991; Keck et al. 2003), when real parts avoid crossing while imaginary ones cross and vice versa, Figure 8(c).

In Figure 9, the "surgery" of eigenvalue branches is clearly seen in the complex (Imλ, Reλ)-plane. Although "on the surface" (for Re(λ) > 0) nothing special happens, the deep reason for the exchange of the fragments between the branches is "hidden" in the Re(λ) < 0 region at some finite value of Pm where an EP is formed, see Figure 9(c). The critical branch (λ_2) that was responsible for SMRI leaves its stable "tail" coming from minus infinity (Figures 9(a) and (b)) and instead "catches" a fragment

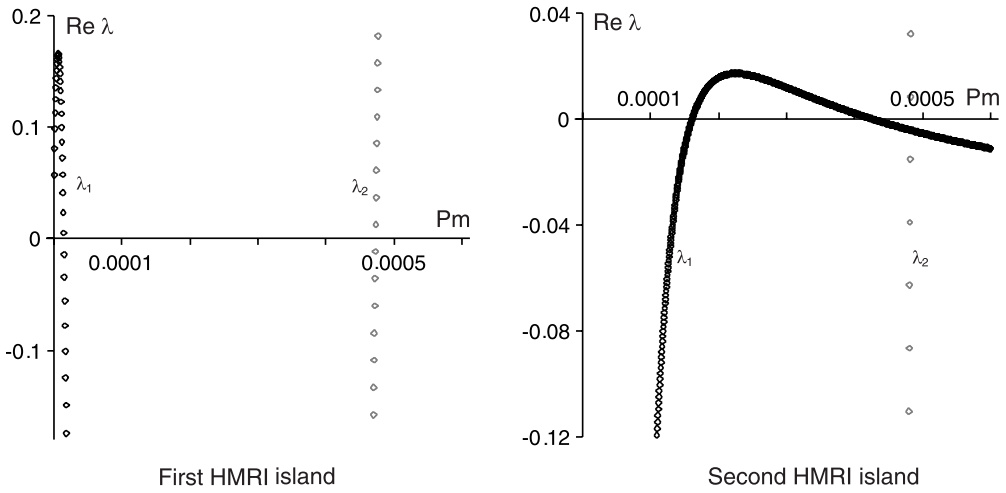

Figure 13. Ha* = 17, Re* = 28850, and Ro = −0.88: (left, $\beta^* = 0.7$) real part of the first critical eigenvalue branch (gray) is positive when Pm is within the continent, while for the second critical branch (black) it is within the first HMRI island; (right, $\beta^* = 2$) real part of the first critical eigenvalue branch (gray) is positive when Pm is within the continent while for the second critical branch (black) it is within the second HMRI island.

of a stable branch of complex eigenvalues (λ_1) with small real parts (Figures 9(d)–(f)). Note that at $\beta^* = 0$ and Pm = 0 we have $\lambda_1 = 0$. This rearranged branch of complex eigenvalues is much more prone to instabilities at low Pm than the original critical one as the further increase of β^* confirms. Indeed, the negative real parts become smaller and around $\beta^* = 0.7$ there appears a new interval of HMRI at those values of Pm, at which SMRI did not exist, see Figure 10(a). This interval exactly corresponds to the island of HMRI shown in Figures 5(b) and (c). We note here that the numerical calculation of the roots of the dispersion relation confirms the boundaries of the regions of HMRI given by the Bilharz criterion: $m_4 = 0$.

The hidden EP governs transfer of instability between the branch of (helically modified) SMRI and a complex branch of the inertial wave that after interaction becomes prone to destabilization. This qualitative effect explains why switching the azimuthal component of the magnetic field on we get HMRI as a traveling wave whereas SMRI was a stationary instability. Moreover, as Figure 10(c) shows, the new critical branch is characterized by a broad band of unstable frequencies while the tail of the branch responsible for SMRI corresponds to a more sharply selected unstable frequency which is close to zero at small $\beta^* \neq 0$, growing, however, up to Im$\lambda \simeq 5$ when β^* is as big as 0.7.

The above observations are in agreement with the observation of Liu et al. (2006) that, in contrast to SMRI, which is a destabilized slow MC wave, HMRI is a weakly destabilized inertial oscillation. Further results on interpretation of the HMRI as an unstable MHD wave as well as on its relation to the dissipation-induced instabilities will be published elsewhere (Y. Fukumoto et al. 2010, in preparation).

4.3.2. Second Scenario of HMRI Excitation

The remarkable complexity of the phenomenon of HMRI manifests itself in different scenarios of destabilization. It turns out that the transition from SMRI to HMRI through an EP is not the only way to instabilities at low magnetic Prandtl numbers. At higher values of Re* and Ha*, in the presence of the azimuthal magnetic field the inertial wave can become unstable without mixing with the critical SMRI branch.

In contrast to the scenario of the first type when one mixed complex branch becomes unstable at different intervals of Pm and causes both the essential HMRI and the helically modified SMRI, in the new situation the inertial wave causes the excitation of the essential HMRI and the critical real branch remains responsible for the helically modified SMRI, as is clearly seen in Figure 11.

Most surprisingly, the inertial wave branch can become unstable twice with the increase of β^*. The first time this happens in the vicinity of $\beta_1^* = \frac{1}{2}\sqrt{2} \simeq 0.707$, see Figure 11(b), then—in the neighborhood of $\beta_2^* = \frac{3}{2}\sqrt{2} \simeq 2.121$, as is visible in Figure 11(c). In the (Pm, β^*)-plane this yields two islands of the essential HMRI that coexist with the continent of the helically modified SMRI, Figure 12(a). The real parts of the unstable branches shown in black and gray in Figure 13 correspond to the first and second essential HMRI islands and to the continent of the helically modified SMRI, respectively.

The difference between the two HMRI scenarios is visible also in the other parameter planes. For example, in (Ha*, Ro)-plane the domain of HMRI developed by the first scenario and corresponding to the HMRI island of Figure 12(c) has an SMRI-like form with two peaks (see Figure 12(d)). The second HMRI excitation scenario can lead to the inclusions of the essential HMRI domain in the domain of the helically modified SMRI (Figure 12(b)). This is natural because the two different eigenvalue branches can be unstable simultaneously at the same values of parameters. Another consequence of the destabilization of the inertial wave without mixing with the critical SMRI branch is that the islands in Figure 12(a) are slices of different three-dimensional domains that can intersect each other along an edge that forms a singularity of the common stability boundary, while the HMRI domains shown in Figure 12(c) are slices of the same three-dimensional region of instability with the smooth boundary, cf. Figure 6(a).

5. CONCLUSIONS

The HMRI is a more complicated phenomenon than the standard one. We found evidences that HMRI can be identified with the destabilization of an inertial wave in contrast to SMRI that is a destabilized slow MC wave. We established two scenarios of transition from SMRI to HMRI. The first one is accompanied by the origination of a spectral EP and a transfer of instability between modes, while in the second scenario two independent

eigenvalue branches become unstable. We distinguish between the essential HMRI that is characterized by small magnetic Prandtl numbers at which SMRI is not possible, smaller growth rates than SMRI, and by non-zero frequencies and the helically modified SMRI which is caused by a small perturbation of the unstable real eigenvalue branch and is thus characterized by high growth rates, small frequency, and relatively high magnetic Prandtl numbers within the usual range of SMRI. With the use of the Bilharz stability criterion we established explicit expressions for the stability boundary and proved rigorously the bounds on the critical Rossby number for HMRI in the inductionless limit (Pm = 0). Nevertheless, we revealed that for Pm ≠ 0 these bounds can be easily exceeded—an indicator in favor of the HMRI for small negative Rossby numbers. Finally, we found that for small negative Rossby numbers the essential HMRI forms separated islands that can coexist simultaneously in the (Pm, β^*)-plane.

The work of O.N.K. has been supported by the research grant DFG HA 1060/43-1. The work of F.S. has been supported by the German Leibniz Gemeinschaft within its SAW program and by DFG in the framework of SFB 609. F.S. also thanks G. Gerbeth, R. Hollerbach, J. Priede, G. Rüdiger, Th. Gundrum, and J. Szklarski for many stimulating discussions.

APPENDIX

LINEARIZATION WITH RESPECT TO NONAXISYMMETRIC PERTURBATIONS

We linearize Equations (1)–(3) in the vicinity of the stationary solution (Equation (4)–(7)) assuming general perturbations $\mathbf{u} = \mathbf{u}_0 + \mathbf{u}'$, $p = p_0 + p'$, and $\mathbf{B} = \mathbf{B}_0 + \mathbf{B}'$ and leaving only the terms of first order with respect to the primed quantities. With the notation (Goodman & Ji 2002; Liu et al. 2006)

$$\partial_t = \frac{\partial}{\partial t}, \quad \partial_\phi = \frac{\partial}{\partial \phi}, \quad \partial_R = \frac{\partial}{\partial R}, \quad \partial_z = \frac{\partial}{\partial z},$$
$$\partial_R^\dagger = \partial_R + \frac{1}{R}, \quad D = \partial_R^\dagger \partial_R + \frac{1}{R^2}\partial_\phi^2 + \partial_z^2 \tag{A1}$$

we write the linearized equations in cylindrical coordinates, cf. Goodman & Ji (2002), Pessah & Psaltis (2005), and Liu et al. (2006):

$$\begin{aligned}
&(\partial_t - \nu D)u'_R - 2\Omega u'_\phi + \Omega \partial_\phi u'_R \\
&\quad = -\frac{1}{\rho}\left[\partial_R p' + \frac{1}{\mu_0}\left(B_z^0 \partial_R B'_z + B_\phi^0 \partial_R B'_\phi - \frac{B_\phi^0}{R} B'_\phi\right)\right] \\
&\qquad + \frac{1}{\mu_0 \rho}\left(B_z^0 \partial_z B'_R + \frac{B_\phi^0}{R}\partial_\phi B'_R - 2\frac{B_\phi^0}{R} B'_\phi\right) \\
&\qquad - \nu\left(\frac{u'_R}{R^2} + \frac{2}{R^2}\partial_\phi u'_\phi\right), \\
&(\partial_t - \nu D)u'_\phi + \frac{\kappa^2}{2\Omega} u'_R + \Omega \partial_\phi u'_\phi \\
&\quad = -\frac{1}{\rho}\frac{1}{R}\left[\partial_\phi p' + \frac{1}{\mu_0}\left(B_z^0 \partial_\phi B'_z + B_\phi^0 \partial_\phi B'_\phi\right)\right] \\
&\qquad + \frac{1}{\mu_0 \rho}\left(B_z^0 \partial_z B'_\phi + \frac{B_\phi^0}{R}\partial_\phi B'_\phi\right) + \nu\left(\frac{2}{R^2}\partial_\phi u'_R - \frac{u'_\phi}{R^2}\right), \\
&(\partial_t - \nu D)u'_z + \Omega \partial_\phi u'_z \\
&\quad = -\frac{1}{\rho}\left[\partial_z p' + \frac{1}{\mu_0}\left(B_z^0 \partial_z B'_z + B_\phi^0 \partial_z B'_\phi\right)\right] \\
&\qquad + \frac{1}{\mu_0 \rho}\left(B_z^0 \partial_z B'_z + \frac{B_\phi^0}{R}\partial_\phi B'_z\right), \\
&(\partial_t - \eta D)B'_R = \frac{B_\phi^0}{R}\partial_\phi u'_R - \Omega \partial_\phi B'_\phi + B_z^0 \partial_z u'_R \\
&\qquad - \eta\left(\frac{B'_R}{R^2} + \frac{2}{R^2}\partial_\phi B'_\phi\right), \\
&(\partial_t - \eta D)B'_\phi = B_z^0 \partial_z u'_\phi - B_\phi^0 \partial_z u'_z - B_\phi^0 \partial_R u'_R - u'_R \partial_R B_\phi^0 \\
&\qquad + u_\phi^0 \partial_R B'_R + u_\phi^0 \partial_z B'_z + B'_R \partial_R u_\phi^0 \\
&\qquad + \eta\left(\frac{2}{R^2}\partial_\phi B'_R - \frac{B'_\phi}{R^2}\right), \\
&(\partial_t - \eta D)B'_z = -B_z^0 \partial_R u'_R - \frac{B_z^0}{R} u'_R - \frac{B_z^0}{R}\partial_\phi u'_\phi \\
&\qquad - \Omega \partial_\phi B'_z + \frac{B_\phi^0}{R}\partial_\phi u'_z, \\
&0 = \partial_R^\dagger u'_R + \frac{1}{R}\partial_\phi u'_\phi + \partial_z u'_z, \\
&0 = \partial_R^\dagger B'_R + \frac{1}{R}\partial_\phi B'_\phi + \partial_z B'_z.
\end{aligned} \tag{A2}$$

REFERENCES

Balbus, S. A. 2009, Scholarpedia, 4, 2409
Balbus, S. A., & Hawley, J. F. 1991, ApJ, 376, 214
Balbus, S. A., & Henri, P. 2008, ApJ, 674, 408
Berry, M. V. 2004, Czech. J. Phys., 54, 1039
Berry, M. V., & Dennis, M. R. 2003, Proc. R. Soc. A, 459, 1261
Bilharz, H. 1944, Z. Angew. Math. Mech., 24, 77
Chandrasekhar, S. 1960, Proc. Natl. Acad. Sci., 46, 253
Dubrulle, B., Marie, L., Normand, Ch., Richard, D., Hersant, F., & Zahn, J.-P. 2005, A&A, 429, 1
Goodman, J., & Ji, H. 2002, J. Fluid Mech., 462, 365
Hollerbach, R., & Rüdiger, G. 2005, Phys. Rev. Lett., 95, 124501
Hollerbach, R., Teeluck, V., & Rüdiger, G. 2010, Phys. Rev. Lett., 104, 044502
Ji, H. T., Burin, M., Schartman, E., & Goodman, J. 2006, Nature, 444, 343
Ji, H., Goodman, G., & Kageyama, J. A. 2001, MNRAS, 325, L1
Keck, F., Korsch, H.-J., & Mossmann, S. 2003, J. Phys. A: Math. Gen., 36, 2125
Kirillov, O. N. 2006, Phys. Lett. A, 359, 204
Kirillov, O. N. 2007, Int. J. Nonlinear Mech., 42, 71
Kirillov, O. N. 2009, Proc. R. Soc. A, 465, 2703
Kirillov, O. N. 2010, Z. Angew. Math. Phys., in press
Kirillov, O. N., Günther, U., & Stefani, F. 2009, Phys. Rev. E, 79, 016205
Kirillov, O. N., Mailybaev, A. A., & Seyranian, A. P. 2005, J. Phys. A: Math. Gen., 38, 5531
Knobloch, E. 1992, MNRAS, 255, P25
Knobloch, E. 2001, Phys. Fluids, 8, 1446
Krechetnikov, R., & Marsden, J. E. 2007, Rev. Mod. Phys., 79, 519
Lakhin, V. P., & Velikhov, E. P. 2007, Phys. Lett. A, 369, 98
Lehnert, B. 1954, ApJ, 119, 647
Lienard, A., & Chipart, H. 1914, J. Math. Pures Appl., 10, 291
Liu, W. 2008a, ApJ, 684, 515
Liu, W. 2008b, Phys. Rev. E, 77, 056314
Liu, W. 2009, ApJ, 692, 998
Liu, W., Goodman, J., Herron, I., & Ji, H. 2006, Phys. Rev. E, 74, 056302
Liu, W., Goodman, J., & Ji, H. 2007, Phys. Rev. E, 76, 016310
Mailybaev, A. A., Kirillov, O. N., & Seyranian, A. P. 2005, Phys. Rev. A, 72, 014104
Marden, M. 1966, Geometry of Polynomials (Mathematical Surveys, Vol. 3; 2nd ed.; Providence, RI: AMS)
Noguchi, K., Pariev, V. I., Colgate, S. A., Beckley, H. F., & Nordhaus, J. 2002, ApJ, 575, 1151

Nornberg, M. 2008, Bull. Am. Phys. Soc., 53, GI2.00003
Nornberg, M. D., Ji, H., Schartman, E., Roach, A., & Goodman, J. 2010, Phys. Rev. Lett., in press
Or, A. C. 1991, Q. J. Mech. Appl. Math., 44, 559
Pessah, M. E., & Psaltis, D. 2005, ApJ, 628, 879
Priede, J., & Gerbeth, G. 2009, Phys. Rev. E, 79, 046310
Priede, J., Grants, I., & Gerbeth, G. 2007, Phys. Rev. E, 75, 047303
Rosner, R., Rüdiger, G., & Bonanno, A., ed. 2004, in AIP Conf. Proc. 733, MHD Couette Flows: Experiments and Models, ed. G. Rosner, G. Rüdiger, & A. Bonanno (Melville, NY: AIP)
Rüdiger, G., & Hollerbach, R. 2007, Phys. Rev. E., 76, 068301
Rüdiger, G., Hollerbach, R., Schultz, M., & Shalybkov, D. A. 2005, Astron. Nachr., 326, 409
Rüdiger, G., Hollerbach, R., Schultz, M., & Shalybkov, D. A. 2008, Astron. Nachr., 329, 659
Rüdiger, G., Hollerbach, R., Stefani, F., Gundrum, Th., Gerbeth, G., & Rosner, R. 2006, ApJ, 649, L145
Rüdiger, G., & Schultz, M. 2008, Astron. Nachr., 329, 659
Sisan, D. R., Mujica, N., Tillotson, W. A., Huang, Y. M., Dorland, W., Hassam, A. B., Antonsen, T. M., & Lathrop, D. P. 2004, Phys. Rev. Lett., 93, 114502
Stefani, F., Gailitis, A., & Gerbeth, G. 2008a, Z. Angew. Math. Mech., 88, 930
Stefani, F., Gerbeth, G., Gundrum, T., Hollerbach, R., Priede, J., Rüdiger, G., & Szklarski, J. 2009, Phys. Rev. E, 80, 066303
Stefani, F., Gerbeth, G., Gundrum, Th., Szklarski, J., Rüdiger, G., & Hollerbach, R. 2008b, Astron. Nachr., 329, 652
Stefani, F., Gerbeth, G., Gundrum, Th., Szklarski, J., Rüdiger, G., & Hollerbach, R. 2009b, Magnetohydrodynamics, 45, 135
Stefani, F., Gundrum, Th., Gerbeth, G., Rüdiger, G., Schultz, M., Szklarski, J., & Hollerbach, R. 2006, Phys. Rev. Lett., 97, 184502
Stefani, F., Gundrum, Th., Gerbeth, G., Rüdiger, G., Szklarski, J., & Hollerbach, R. 2007, New J. Phys., 9, 295
Szklarski, J. 2007, Astron. Nachr., 328, 499
Tayler, R. J. 1973, MNRAS, 161, 365
Umurhan, O. M. 2006, MNRAS, 365, 85
Velikhov, E. P. 1959, Sov. Phys.—JETP, 36, 995
Wendl, M. C. 1999, Phys. Rev. E, 60, 6192